Deforming Grid Generation and CFD analysis of Variable Geometry Screw Compressors

Sham Rane*, Ahmed Kovacevic, Nikola Stosic, Madhulika Kethidi
Centre for Positive Displacement Compressor Technology,
City University London, EC1V 0HB, London, U.K. email: sham.rane.1@city.ac.uk * Corresponding Author
Tel: +44(0) 20 70408395, Fax: +44(0) 20 70408566

Abstract

The most common type of twin screw machines are twin screw compressors. These normally contain rotors of uniform pitch and profile along the rotor length. However, in some cases such as in twin screw vacuum pumps with very large pressure ratios, the variable pitch rotors are often used to improve efficiency. The limited use of rotors with variable pitch and/or section profile is mainly due to manufacturing constraints. In order to analyse the performance of such machines by means of Computational Fluid Dynamics (CFD), it is necessary to produce a numerical mesh capable of calculating 3D transient fluid flows within their working domains.

An algebraic grid generation algorithm applicable to unstructured grid, Finite Volume Method (FVM) for variable pitch and variable profile screw machines is described in this paper. The grid generation technique has been evaluated for an oil free air compressor with "N" profile rotors of 3/5 lobe configuration. The performance was obtained by calculations with commercial CFD code. The grid generation procedure provides mesh of the required quality and results from CFD calculations are presented to compare performance of constant pitch rotors, variable pitch rotors and variable profile rotors. The variable pitch and variable profile rotors achieve steeper internal pressure rise and a larger discharge area for the same pressure ratio. Variable Pitch rotors achieve reduced sealing line length in high pressure domains.

Keywords: Algebraic Grid Generation, Computational Fluid Dynamics, Twin Screw Compressor, Variable Pitch Rotors, Variable Profile Rotors.

Nomenclature:

L – Rotor Length

D – Male Rotor Outer Diameter

Φ_w – Male Rotor Wrap Angle

α – Male rotor rotation angle

$\Delta\alpha$ – Increment in Male rotor rotation angle

Z – Axial distance along the rotors

ΔZ – Increment in Axial distance

z_1 – Number of lobes on the Male rotor

z_2 – Number of lobes on the Female rotor

i – Rotor Gear ratio = z_2/z_1

p_s – Starting Lead

p_e – Ending Lead

j_a – Grid density in axial direction per interlobe

x – X coordinate

y – Y coordinate

r – Radius

θ – Angle turned by male rotor

r.p.m – Male rotor speed

t – Time

Δt – Time Step Size

V_i – Built in Volume Index

Abbreviations:

CFD – Computational Fluid Dynamics

FVM – Finite Volume Method

SCORG – Screw Compressor Rotor Grid Generator

PDE – Partial Differential Equation

TFI – Transfinite Interpolation

GGI – Generalized Grid Interface

1 Introduction

Screw compressor rotors are effectively helical lobed gears with profiles developed for optimized compression process. The compressor working chamber is formed by the space contained between the intermeshing rotors and the casing which decreases is size as they rotate. Fig. 1 shows an example of a CAD model of an oil free twin screw compressor in which the

compression process, leakage flows, heat transfer, oil injection and other phenomena of interest for compressor design occur within that space. To achieve efficient compression the clearances between the rotors and between the rotors and the casing must be minimised. For oil injected compressors these can be as small as 40 μm but for dry compressors these may have to be of the order of hundreds of micro meters to allow for thermal expansion. Regardless of the type of compressor and depending on the size of the machine, the working chamber main dimensions can be of the order of 1000 times larger than these values. This complicates the task of creating numerical meshes capable of such a dimensional variation. This is further exacerbated by the transient nature of the process, high pressure and temperature gradients, and domains with a variety of flow regimes.

Fig. 1. Oil free Twin Screw compressor and its working chamber

Grid generation for numerical simulation of 3D flow processes requires the domain to be broken up into a number of regularly shaped discrete volumes with computational points in the centre of each. In order to obtain boundary conformal representation of physical space, most grid generation techniques start from the boundaries and proceed to the interior. There are three main classes of mathematical techniques used for this process, a) Algebraic methods, b) Differential Methods and c) Variational methods. Authors such as [*20, 29, 30*] have described different grid generation techniques in detail. Shih et al [*24*] reviewed different types of grids and their relative advantages.

Algebraic methods are direct and depend on the use of parametric functions to discretize the boundaries and then use interpolation to calculate interior points. They are suitable for regular geometries and structured grids and have relatively simple implementation. Numerical grids are obtained quickly by these methods with good control over their distribution. [*2, 3, 9, 19, 23, 24,*

25, 26] have described various aspects of algebraic grid generation such as the control point form, transfinite interpolation techniques, grid adaptation, weighting functions for multivariable adaptation etc.

Differential methods are indirect and more suitable for complex geometries. They depend on the solution of partial differential equations. These can be elliptic, parabolic or hyperbolic in nature and their selection depends on the geometry to be discretized. Boundary discontinuities can be avoided to extend to the interior points, but they require significant computational effort and time to solve.

Variational methods depend on such measures of the grid quality as orthogonality and skewness. Using them, the computational points can be distributed to optimize a function of the grid quality. However, they have complex formulations and are difficult to control.

Methods for grid generation in screw compressor applications need to be easy to implement and quick. Analysis of the working chamber is transient in nature and requires a grid to represent a rotor position for every time step, taking into account the change in size of the working domain. In this respect, algebraic methods can recalculate the grid quickly. In [*10, 11*], *Kovacevic et. al.* have successfully used an algebraic grid generation method together with boundary adaptation and transfinite interpolation. This has been implemented in the custom made program for the calculation of a screw compressor numerical mesh called SCORG. *Kovacevic* in [*16*] presented the grid generation aspects for twin screw compressors in detail. In [*12, 13, 14, 15, 17* and *18*], *Kovacevic et. al.* have reported CFD simulations of twin screw machines for the prediction of flow, heat transfer, fluid-structure interaction, etc.

The use of a differential method requires the solution of a PDE for every rotor position. The grid generation calculation has then to be repeated from equipotential and gradient lines of the

solution. Also there is little control available for the solution of these PDE's. *Voorde et. al.* in [*31, 32*] developed an algorithm for conversion of an unstructured grid to a block–structured mesh for twin screw compressors and pumps from the solution of the Laplace equation. Apart from these works, there are only a few reports available on transient three dimensional CFD analyses of screw machines. All these developments were concentrated on machines with uniform pitch rotors and so far no published work is available on the numerical analysis of twin screw compressors with variable pitch or variable profile rotors.

The use of general purpose grid generators for screw compressors has been found to be inadequate [*18, 21, 22*] and only customized grid generation programs are available for twin screw compressor applications. The motivation for the present work was to develop existing functionality to handle grid generation of twin screw rotors with variable pitch and variable section profiles so that CFD simulations of these new types of machines is possible.

Numerical treatment of the CFD models for screw compressors with uniform lead and variable lead rotors differs mainly at the grid generation stage. In the grid generation technique for constant pitch rotors the axial distance between the grid points is constant. The challenge in generating a grid for variable lead rotors is that the axial distance and angular rotation of nodes change continuously. To accommodate this change, the grid needs variable spacing in the axial direction which will still provide a conformal mesh. This topology remains the same over the entire length of the rotor but the rotors change their relative position governed by the variable lead. Apart from that, the grid generator has to accommodate the large difference in length scales of the main domain and the clearances.

2 Uniform versus Variable Pitch

Although there is a patent by *Gardner* [*7*] on continuously variable pitch rotor dated back to 1969, such machines are not used much and are still in the research phase. The patent proposes a helical screw compressor with continuously variable lead for both rotors, male and female. Due to the lack of manufacturing techniques to produce such rotors, Gardner proposed forming them from a stack of metal plates with different leads which is still used today in some designs of vacuum pumps. Fig. 2 shows twin screw rotors with uniform pitch whereas Fig. 3 shows twin screw rotors of the same size but with variable pitch. It has been shown in literature that for the same rotor lengths, diameter, wrap angles and lobe profiles, variable pitch rotors can be designed to provide higher pressure ratios and larger discharge port opening areas with reduced throttling losses when compared to constant pitch rotors [*7*].

Fig. 2. Meshing of Uniform Pitch Twin Screw Rotors

Fig. 3. Meshing of Variable Pitch Twin Screw Rotors

As confirmed by many authors, screw compressor efficiency depends upon the profile of the rotors, the combination of male and female lobes, the length and diameter, the wrap angle and the rotor clearances [*5, 6, 8*]. Based on these and the original work of *Gardner* [*7*] it is suggested that the effects of variable lead rotor designs are as follows;

a) If all other variables are unchanged for a constant lead rotor pair and a variable lead rotor pair, the length of the sealing line will be less for the variable rotor pair as the rotor lead reduces from suction to discharge. Since the leakage loss is directly proportional to the length of the sealing line and the sealing line is shorter for the variable lead rotors in the

high pressure regions, the leakage loss will be reduced. This may lead to higher volumetric efficiencies with variable lead rotors.

b) For variable lead rotors, the reduction of volume during the compression process will be faster than for constant lead rotors, as shown in Fig. 4. Consequently the pressure will rise more rapidly for the variable lead rotors as shown in Fig. 5.

c) The built-in volume index is the ratio of the suction closure to the discharge opening volumes. The suction volume is the maximum volume at which the suction port is usually closed and where the compression process begins. The discharge volume is the size of the compression chamber at the moment of opening of the discharge port. As shown in Fig. 4, to achieve the same V_i for variable pitch rotors the discharge port should be opened earlier which allows it to be bigger than in the constant lead case. Hence it is possible to have a greater discharge area at a similar pressure ratio and this will reduce the throttling losses. Fig. 6 shows the radial and axial ports for the variable and constant lead rotors in order to demonstrate the difference in size of the ports with the same V_i and discharge pressure.

Fig. 4. Volume-Angle diagram

Fig. 5. Pressure-Angle Diagram

d) If the same size of discharge port is retained for both the variable and uniform lead rotors, the discharge pressure of the variable rotors will be higher. This indicates that variable lead rotors can achieve a higher V_i index.

Fig. 6. Cylinder and Port development of a rotor pair

However, a variable lead compressor with the suction port in the same position as in a uniform lead compressor may have a reduced capacity.

The advantages and disadvantages identified on the basis of previous research have not been tested so far on physical prototypes due to difficulties in producing such rotors with existing manufacturing methods. However, these can be investigated further in detail by use of CFD analysis if an appropriate numerical mesh can be generated. The arguments b, c and d presented above are applicable even for variable profile rotors designed such that the flow area is reduced continuously from the suction to the discharge end of the rotors.

3 Grid Generation for uniform pitch screw rotors

The screw compressor working domain is spatially discretized by use of both, structured and unstructured grids. The flow domains of the screw compressor consist of the rotor domain, the suction port and the discharge port.

Fig. 7. Twin screw compressor working chamber domains

Fig. **7** shows a complete grid of the compressor model. The suction and discharge ports can be meshed by use of general purpose grid generators in which case it is easier to generate a tetrahedral unstructured grid with fine prism layers covering the boundaries. The customized grid generator [*18*] is used for the generation of a structured hexahedral mesh consisting of two sub-domains each belonging to one of the rotors. The rotor mesh changes for every time step, causing deformation of the generated finite volumes and sliding on the interfaces. The sole reason for the use of the customized grid generator for a screw compressor is that unstructured meshes do not provide a fully conserved solution and this is unacceptable for the evaluation of screw

compressors [*22*]. These tetrahedral meshes of the ports and the hexahedral meshes of two rotor subdomains are connected by non-conformal GGI interfaces in the solver.

Fig. 8. Simplified Block Diagram of Screw Compressor Rotor Grid Generator

Hexahedral meshes for the rotor domains are generated by the use of an algebraic grid generation method employing multi parameter one dimensional adaptation and transfinite interpolation. Fig. 8 shows a simplified block diagram of the steps performed in the screw compressor rotor grid generator. The topology of the flow domain between the male rotor, female rotor and the casing resembles a ∞ figure. In order to simplify the grid generation process, the entire rotor domain is subdivided in two regions each belonging to one of the rotors. These domains are separated by the rack, a curve which uniquely separates both domains [*27*]. By this means an "O" grid is constructed for each rotor domain.

Consecutive 2D cross sections are calculated individually using the following steps [16]:

- Transformation from the 'physical' domain to the numerical domain.
- Definition of the edges by applying an adaptive technique.
- Selection and matching of four non-contacting boundaries.
- Calculation of the curves, which connect the facing boundaries by transfinite interpolation.
- Application of a stretching function to obtain the distribution of the grid points.
- Orthogonalisation, smoothing and final checking of the grid consistency.

This procedure is the most important function of the framework and provides flexibility to extend the framework to more complex rotor designs like variable pitch or variable profiles.

The rack generation procedure, using a primary curve to specify both rotor profiles, is described in detail by *Stosic* in [*27, 28*].

With reference to Fig. 9, the interlobe angle is the angle which the male rotor needs to rotate to get one lobe in the position of the next one. This angle is equal to $2\pi / z_1$. The interlobe angle of the female rotor is proportional to the male interlobe angle by the ratio of z_1 / z_2. After each interlobe angle rotation, the rotors come into geometrically identical position to the starting position. Hence the grid vertex positions can be reset to the starting position after each interlobe angle rotation and renumbered, as required, to maintain progressive rotation. Similarly the same set of generated cross sectional meshes can be repeated along the rotor axis with appropriate renumbering of the nodes and cells. Angular rotation of the rotor covering one interlobe angle is discretized into j_a divisions and each angular increment is then equal to $\Delta\alpha = (2\pi / (j_a \ z_1))$. This angular increment is the governing factor for the size of the time interval in a transient simulation. The 2D grids for each of cross sections are generated using the above principle and the functionality shown in flow chart Fig. 8 and are stored in the vertex coordinate files.

Fig. 9. Uniform Pitch Grid Generation

Due to the constant helix angle the axial distance between cross sections corresponds to the angular rotation of the rotor. As shown in Fig. 9, one interlobe angle corresponds to the axial rotor length of one pitch. Due to this correlation the structure of 3D data will consists of repeating blocks of data with updated indexing of the vertices which are generated only once for the first interlobe. During this stage, the hexahedral cell connectivity will also be established for the first generated section by use of 4 nodes from one cross section and the remaining 4 nodes from the neighbouring section. All other axial grid sections will be repeated and equally spaced into $Z_n = \Phi_w / \Delta\alpha$ number of sections.

Transient simulation of the fluid flow requires that the external mesh, representing the domain for all time steps is available and the appropriate mesh is imported in the solver at the beginning of each time step. This process is shown in the block diagram in Fig. 10. The mesh representing the initial position is written with all data for Z_n numbers of sections. For the next time step, the grid is re-indexed so that the cross sections are moved for one ΔZ interval and the front cross section is stacked at the end position. In other words, this is achieved by re-indexing the nodes for all the cross sections so that indices of the previous section are associated with the next one taking all into account, from the first to the last section.

Since all cross sections are at the constant distance ΔZ the fixed angular increment $\Delta\alpha$ will represent constant rotational speed. The time step size for the entire simulation is constant and defined as $\Delta t = 60.0/ (\text{rpm } j_a z_1)$.

Fig. 10. Uniform Pitch Rotor Grid Assembly in 3D

4 Grid Generation for variable pitch and variable profile screw rotors

For the Uniform Pitch rotors, there is a fixed relation for the axial distance between the cross sections and the unit rotation angle over the entire length of the rotor. This is convenient because the profile is constant and the grid generated for one interlobe space can be reused in consecutive interlobes. However, for rotors of variable pitch, this relation varies along the length of the rotor. Therefore it is impossible to use the same method with a constant axial distance between sections for grid generation of such rotors. At the same time the rotors need to rotate at a constant angular speed similar to the rotors of constant pitch. In such a case the angular and axial intervals for grid definition do not relate directly to the angular rotation. Fig. 11 shows the grid difference between the constant and variable pitch rotors.

Fig. 11. Axial spacing difference between uniform pitch and variable pitch rotor grids

Fig. 12. Twin screw compressor rotor with variable section profile

The situation is even further complicated if the rotors have variable section profile along the rotor length as shown in Fig. 12 as an example of twin screw compressor rotors. In that case not only the data structure changes, but also the grid distribution varies from one section to the other. In order to incorporate these variations into the grid generation, the functionality and methodology of data structure generation must be modified and made adaptable for variable pitch and/or variable profile rotors.

In order to achieve this, the existing structure of the procedure used in SCORG has been reformulated to be adaptable with the variable pitch and variable profile screw rotors. The main program has both functionalities of the fixed and variable pitch rotors while the later one is branched either into the uniform profile or the variable profile. The variable profile and variable pitch rotor is geometrically the most difficult and computationally more expensive gradually reducing in complexity to the existing uniform pitch rotors.

However, the functionality presented in the flow chart shown in Fig. 8 does not change even for the most complex case and is used to generate the cross section grids for each time step. The generated data are arranged in a different manner which allows for pitch variation while the repeated generation of data is required in the case of variable profile for each cross section.

The pitch variation could be constant, linear or stepped. The former is used in screw vacuum pump technology while the latter is applicable for some car superchargers. Fig. 13 shows how

the angular rotation of consecutive sections varies with the axial distance for different types of Pitch functions. The expressions used for these functions are specified in equations 1 – 3.

Constant Pitch

$$\mathbf{p = constant} \tag{1}$$

Linear Pitch

$$\mathbf{p} = \left(\frac{\mathbf{p_e - p_s}}{\mathbf{L}}\right)\mathbf{z} + \mathbf{p_s} \tag{2}$$

Quadratic Pitch

$$\mathbf{p} = \left(\frac{\mathbf{p_e - p_s}}{\mathbf{L^2}}\right)\mathbf{z^2} + \mathbf{p_s} \tag{3}$$

As seen from Fig. 13, for a given rotor length the wrap angle can be altered by varying the pitch. In this example the medium pitch is 35.23 mm for which the wrap angle is 300°. Linear variation from an initial pitch of 50.46mm to a final pitch of 20.00mm, which has the same medium pitch, will increase the wrap angle to 461° while a quadratic variation will increase it to 402°. If the wrap angle is kept constant at 300°, the length of rotor with linear pitch variation will be 25% shorter than that with constant pitch. For a quadratic function this change will be smaller. This might be an advantage in screw machines such that for the same wrap angle, the compression process caused by the steeper reduction of volume will be faster and the discharge port opening can be positioned earlier, in turn increasing the discharge port area. This could reduce throttling losses in the discharge port.

Two approaches are proposed here to the solution of grid generation for the CFD analysis of such machines. Approach 1 is easier to implement by modifying the existing procedure and is suitable for variable pitch machines with a uniform rotor profile. Approach 2 is more complex in nature but is generally applicable for any cross section, including those of conical rotors or single screw machines.

Fig. 13. Angular rotation of sections for different Pitch Functions

4.1 Approach 1

In this approach, the pitch function is used to derive a relationship between the fixed angular increments $\Delta\alpha$, from one section to the other and the required variable axial displacements ΔZ_1, ΔZ_2, ΔZ_3…. ΔZ_n for each cross section of the rotor. By this means, the grid vertex data generated for one interlobe angle are reused and positioned in the axial direction with variable ΔZ which conforms to the pitch variation function.

A sample formulation of an axial displacement function for linear pitch variation is shown below. The objective is to find the axial position of the current rotor section, such that it is offset by a fixed angular rotation $\Delta\alpha$ from the previous section.

Current section angle $= \alpha_i$ deg

Axial position $= Z_i$ m

Previous section angle $= \alpha_{i-1}$ deg

Axial position $= Z_{i-1}$ m

$(\alpha_i - \alpha_{i-1})$ = fixed $\Delta\alpha = \frac{2\pi}{z_1 j_a}$ …… Fixed Angular offset (4)

If p_s and p_e are starting and ending lead values and z_1 is number of lobes on male rotor then for the current section, locally lead will be

$$p_i = \left(\frac{(p_e - p_s)}{L}\right) Z_i + p_s \quad \text{..... Linear Variation} \quad (5)$$

Locally, angle per unit length = $2\pi / p_i$

Current section angle is,

$$\alpha_i = \alpha_{i-1} + \frac{2\pi}{p_i}(Z_i - Z_{i-1}) \quad (6)$$

$$(\alpha_i - \alpha_{i-1}) = (Z_i - Z_{i-1})\frac{2\pi}{p_i}$$

$$Z_i = Z_{i-1} + \frac{\left(\frac{(p_e - p_s)}{L}\right)(\alpha_i - \alpha_{i-1})}{2\pi} Z_i + \frac{p_s\,(\alpha_i - \alpha_{i-1})}{2\pi} \quad \text{..... From (5)}$$

$$Z_i \left[1 - \frac{\left(\frac{(p_e - p_s)}{L}\right)(\alpha_i - \alpha_{i-1})}{2\pi}\right] = Z_{i-1} + \left[\frac{p_s\,(\alpha_i - \alpha_{i-1})}{2\pi}\right] \quad (7)$$

Equation 7 is used to find out the axial position of each of the sections over the rotor length. Additional computational effort is required compared to the uniform pitch rotors to calculate this axial position of cross sections. The assembly of a grid from a 2D to a 3D structure remains the same expect for the z coordinates. But this approach cannot be used if there is any variation in the section profiles of the rotor.

4.2 Approach 2

This approach addresses the more generic requirement for the rotor pitch variation along with a variable cross section profile over the length of the rotor. Hence in addition to the axial variation of cross section as done in approach 1 to accommodate pitch variation, the algorithm needs a facility to capture the variation in the cross sections.

The grid generation algorithm is represented in a block diagram in Fig. 14. The foundation of the approach is that every cross section of the screw compressor rotor is a conjugate profile pair. So every cross section can be handled independently and the grid generation process of the flow chart in Fig. 8, from the splitting of the rotor domain by a rack to the allocation of 2D vertex coordinate data can be repeated with the SCORG subroutines.

The process starts with the division of the rotor length into a number of cross sections and proceeds with the generation of 2D vertex data in the first cross section. At this stage the entire procedure shown in Fig. 8 is utilized, the profiles are generated to cover one entire interlobe angle and at corresponding positions, the rack is calculated. This is followed by the boundary discretization and adaptation. Interior nodes at this section are calculated using transfinite interpolation and the vertex data are recorded after the grid orthogonalisation and smoothing operations. This step is labelled as Subroutine run 1 in the block diagram Fig. 14 and generated data are stored as vertex coordinate data.

The next step is a repetition of the process over the second cross section and ends with the generation of 2D vertex data covering one interlobe angle in this second section. Additionally this section receives its axial position from the axial function as described in *Approach 1*. 2D grid generation is completed over all the cross sections, after which the data are used to assemble a set of grid files representing the rotor domain for each time step. Fig. 15 shows the block diagram of the mesh assembly algorithm. At the end of the 2D grid generation, each section has vertex positions for a number of rotor positions covering one interlobe angle. From each section a block representing the first rotor position is collected and transferred to the 3D grid matrix with the correct z coordinate variation. These data are recorded as the first mesh. Then the second block of data is collected and used to build the second mesh. This is repeated for one interlobe angle.

Fig. 14. Variable Pitch and Variable Profile Grid Generation

Fig. 15. Grid Assembly in 3D for Variable Pitch and Variable Profile rotors

After one interlobe angle, the rotors return to the geometrical position identical to that at the start, so the first vertex coordinate data block from every section are again collected and when building the 3D mesh care is taken to re-index the nodes correctly such that the rotor position gets an increment of One Interlobe + $\Delta\alpha$ angle and does not instead return to the starting position. After one complete cycle of intermeshing of the rotor, which is given by (j_a z_1 z_2) meshes, the grid truly returns to its original position.

4.3 Grid Generation examples for variable pitch and uniform profile

As an example of grid generation with variable pitch and uniform section, a 5/6 lobe combination compressor with 'N' rotor profiles was generated. The original rotor design was with an L/D ratio of 1.65, wrap angle of 300° and a rotor length of 210.25 mm.

Fig. 16. Examples of a variable pitch grid with a uniform profile on 5/6 'N' rotors

Approach 1 was used and three sets of grids were generated as shown in Fig. 16. In all of the grids, the node density in all the circumferential, radial and axial directions was maintained the same. The first grid is with a uniform pitch, the second is with a linear pitch variation such that the starting pitch is the same as that of the uniform rotors but it ends with a low pitch of 20.00 mm. This variation gives an increased wrap angle of 425°. The third example is where the initial pitch is high at 80.00 mm and the final pitch is low at 20.00 mm. This variation gives a wrap angle of 340°, close to the uniform pitch rotors. The examples shown for variable pitch in Fig. 16 are to demonstrate the grid generation capability although this high level of variation may not be ideal for compressor rotor designs.

4.4 Grid Generation examples for uniform pitch and variable profile

As an example of grid generation with uniform pitch and variable section, a 3/5 lobe combination compressor with 'Rotor Generated N' profiles was generated. The original rotor design was with an L/D ratio of 1.7, wrap angle of 306° and a rotor length of 230.775 mm.

Fig. 17. Example of a uniform pitch grid with a variable profile on 3/5 'Rotor Generated N' rotors

Approach 2 was used and a set of grids was generated as shown in Fig. 17. In all of the grid sections, the node density in all the circumferential, radial and axial directions was maintained the same. The cross sections changes continuously from suction end to the discharge end of the rotors. As the centre distance is fixed, the rotors are of parallel axis and a tapered shape. The outer diameter on the main rotor is tapered while the inner diameter is constant while on the gate rotor, the inner diameter is tapered and the outer is constant.

Fig. 18. Grid sections of variable geometry on 3/5 'Rotor Generated N' rotors

Fig. 18 shows the 2D cross sections grids for variable rotor profile at the suction end, middle of the rotors and the discharge end.

5 CFD Analysis

The numerical analysis was carried out with the objective of validating the new grid generation procedures and to study the flow behaviour in variable geometry screw compressors.

The test case is an oil free twin screw compressor. Male rotor has 3 lobes with 127.45mm outer diameter, L/D ratio 1.6 and wrap angle Φ_w of 285°. The female rotor is with 5 lobes and the rotor

to rotor centre distance is 93mm. Rotors are rack generated ‘N’ profiles. The compressor speed is 8000 rpm with pressure ratio of 2.0 and 3.0. Four test cases were calculated.

Case 1. Uniform pitch and uniform profile rotors with built in volume index V_i of 1.8.

Case 2. Uniform Pitch and Profile rotors with a reduced discharge port opening area to give a built in volume index V_i of 2.2. In this case, the compression chamber is exposed to the discharge pressure relatively late in the cycle as shown in Fig. 19 and allows for further pressure build up in the chambers.

Fig. 19. Reduced discharge port area in *Case 2* compared with *Case 1*

Case 3. Variable pitch with uniform profile rotors and built in volume index V_i > 1.8. The Suction side pitch was 130mm and Discharge side pitch was 40mm. The wrap angle of Φ_w 285° was maintained as shown in Fig. 20.

Fig. 20. Variable pitch grid – 3/5 ‘N’ rotors

Case 4. Variable profile and uniform pitch rotors. Rotor profile in successive sections is generated using rack generation procedure by variation of addendum on the defining racks [28]. Addendum on the suction end of the rotors was 33mm while on the discharge side it was reduced to 21mm. The addendum on the uniform profile rotors had constant value 28.848mm. Due to the variation of addendum the outer diameter of the male rotor is changing while the inner diameter remains constant and vice versa for the female rotor as shown in Fig. 21. The displacement of these rotors is smaller than for the uniform profile rotors.

Fig. 21. Variable profile grid – 3/5 ‘N’ rotors

Each rotor configuration was analysed on three levels of successive grid refinements. Table 1 shows the number of computational nodes in each case. Stationary compressor ports were meshed by use of the commercial grid generator. Fig. 7 shows the different parts of the numerical model and the grid refinement is shown in Fig. 22. The numerical solver used for the study was ANSYS CFX [*1*], which uses a vertex-based Finite Volume Method and iteratively solves for momentum and continuity in a pressure coupled algorithm. All the generated grids are passed to the solver in the model setup and during solution the rotor domain grids were updated for every time step using external subroutines. The space conservation law is retained during this grid motion by modifications to the governing equation as described by *Ferziger* and *Peric* in [*4*]. The solver was set with a *Higher Order* advection scheme and a *Second Order Backward Euler* temporal discretization.

Fig. 22. Different level of grid refinements shown for one section

Table 1. Grid refinement as number of computational nodes

The boundary conditions at the suction and discharge of the compressor are highly unsteady and therefore difficult to specify. To provide good boundary conditions, the ports were reasonably extended to get good convergence of the flow and reduce the numerical discrepancies arising from pressure pulses in the flow. The working gas was air with an equation of state defined by the Ideal gas law for density. The suction receiver pressure was 1.0bar absolute and the Discharge receiver pressure was 2.0bar and 3.0bar absolute. The convergence criteria for all equations were targeted at $1.0x10^{-3}$ and the coefficient loops for every time step were set at 10. During the solution, the rms residuals for all the time steps were between $1.0x10^{-3}$ and $5.0x10^{-3}$ for the momentum equation and below $1.0x10^{-3}$ for the continuity and energy equations. The

calculations were run until cyclic repetition of the flow and pressure characteristics were identified at the boundaries. Each case was calculated with both Laminar and SST k-Omega Turbulence model.

5.1 Results and Discussion

5.1.1 Compression characteristics

Fig. 23 shows the variation of pressure in case of variable pitch rotors. Fig. 24 shows the compression characteristic of cases 1, 3 and 4 for one full cycle on fine grids with discharge pressure of 2.0bar. With uniform rotors the maximum internal pressure goes up to 2.5bar and with variable geometry rotors the maximum internal pressure goes up to 3.0bar. *Case 3* with the variable rotor pitch and *Case 4* with variable rotor profile have a steeper rise in internal pressure than *Case 1* which has constant rotor geometry. The highest peak pressure is achieved with the variable pitch rotors. For a discharge pressure of 2.0bar this internal pressure rise is a condition of over-compression.

Fig. 23. Pressure variation on variable pitch medium grid case with discharge pressure 2.0bar.

Fig. 24. Indicator diagram for cases calculated on fine grid. Discharge pressure 2.0 bar.

Fig. 25 shows the compression characteristic of the four cases on fine grids with discharge pressure of 2.0bar and 3.0bar and SST k-omega turbulence models. Uniform rotors show high under compression and with variable geometry rotors the maximum pressure goes up to 3.4bar.

Fig. 25. Indicator diagram for cases calculated on fine grid with turbulence models. Discharge pressure 2.0bar and 3.0 bar.

5.1.2 Discharge Port Area

Fig. 19 shows a decrease in the discharge port area with the increased V_i to 2.2. In *Case 2*, with uniform pitch and a reduced discharge port opening area, the internal pressure rise was about

3.1bar before exposure to a discharge pressure of 2.0bar as seen in Fig. 25. This pressure rise was close to that of the variable geometry rotors of about 3.0bar, for which the opening area was 22% higher. The increment in the discharge area for comparable pressure rise is favourable to the reduction of throttling losses in the compressor.

5.1.3 Influence of grid refinement

Fig. 26 shows the effect of grid refinement on the prediction of integral quantities such as the mass flow rate, indicated power and specific power for cases 1, 3 and 4 with 2.0bar discharge pressure. The mass flow rate showed an increase with grid refinement in all cases. The difference between each consecutive grid refinement is around 10%.

Fig. 26. Effect of grid refinement on integral parameters in cases 1,3 and 4 with 2.0bar discharge pressure

This indicates that the rotor geometry is captured better with finer grids, which results in reduction of leakages. Similarly, indicated power increases by 2-5% each time the grid is refined. The increase in the chamber pressure with grid refinement is shown in Fig. 27 for the *Case 4* with variable profile rotors as an example.

Fig. 27. Indicator diagram for cases 4 showing effect of grid refinement with 2.0bar discharge pressure

5.1.4 Influence of Turbulence Model

As shown in Fig. 26, higher mass flow rates are achieved when the turbulence model is applied. Indicated power also increases as the consequence of increased mass flow. However, specific power is reduced for all turbulent cases indicating that influence of turbulence models on mass flow rate prediction is higher than that on indicator diagram/power prediction.

5.1.5 Sealing Line Length

The interlobe sealing line is the line of closest proximity between the two rotors. The leakage of gas takes place through this gap and is proportional to the length of the sealing line and clearance normal to it [*5, 6, 8*]. Contours of pressure distribution on the rotors can be established from

numerical calculations and the dividing line between high and low pressure levels can be considered as the sealing line. The maximum pressure gradient is present across this division and is the driving force for leakage.

Fig. 28. Comparison of interlobe sealing line lengths

Fig. 28 shows the sealing lines obtained on the uniform pitch rotors (*Case 1)* and variable geometry rotors (*Case 3* and *Case 4*). The projection of the sealing line on the rotor normal plane shows the difference more clearly. The sealing line on the uniform pitch rotor is of the same length for each interlobe space along the rotor. However, on the variable pitch rotors the sealing line is longer at the suction end. It decreases towards the discharge end of the rotor.

Table 2. Comparison of Interlobe Sealing Line Length [mm]

Table 2 presents the variation in the sealing line lengths between the uniform and variable geometry cases at one of the rotor positions indicating the magnitude of change along the rotors. At the suction end the sealing line on variable pitch rotor is 30mm longer but at the discharge end it is 12mm shorter. This helps to reduce leakage as the largest pressure difference across the sealing line is at the discharge. Additionally, the total length of the sealing line is reduced by 11mm in the variable pitch rotors. In *Case 4* with variable profile the suction end is longer by 12mm and discharge end has very small difference compared with the uniform profile. There is no overall gain in sealing line length because of the increased gate lobe thickness near the discharge end of the rotors.

5.1.6 Blow-hole area

Blow-hole area is the leakage area formed between the male and female rotors and the casing at the rotor cusp as shown in Fig. 29. The blow-hole area on the high pressure side is important for

leakage due to the pressure difference between adjacent compression chambers. A smaller blow-hole area is desired for improved performance of the machine. Table 3 shows the blow-hole areas measured on the medium size grid for different calculated cases at three positions on the rotor.

Fig. 29. Comparison of Blow-hole area

Table 3. Comparison of Blow-hole area [mm^2]

The blow-hole area for the uniform rotors remains constant along the length of the rotors. In the variable pitch rotors, the suction side blow-hole area is larger than in the uniform rotors but the discharge side blow-hole area is smaller than for the uniform rotors. In the variable profile rotors, the suction side blow-hole area is nearly the same as that of the uniform rotors but the discharge blow-hole area is smaller than for the uniform rotors. Proportionally, the reduction of blow-hole area towards the discharge side rotors is most pronounced in the case of variable pitch rotors.

5.1.7 Overall performance

The influence of the discharge pressure on the compressor performance for the analysed cases 1, 3 and 4 is shown in Fig. 30. Uniform rotors have a highest flow rate and lowest specific power for both pressures. However the difference in the specific power between uniform and variable geometry rotors is much reduced at higher pressures.

Fig. 30. Comparison of performance at 2.0bar and 3.0bar discharge pressure with fine grid cases

Table 4. Comparison of predicted variable geometry rotor efficiencies

Table 4 shows the comparison of predicted volumetric and adiabatic efficiencies. Uniform rotors show highest volumetric efficiency at 2.0bar. But with V_i 2.2 the efficiency is lower than that of variable pitch rotors due to comparable internal pressure rise and comparatively shorter sealing

line length in variable pitch rotor. Also variable pitch rotors have higher volumetric efficiency at 3.0bar discharge pressure.

Uniform rotors show highest adiabatic efficiency at 2.0bar. But with V_i 2.2 the efficiency is lower than that of variable geometry rotors. At 3.0 bar discharge pressure variable geometry rotors have equivalent adiabatic efficiency with uniform rotors and higher than their efficiencies at 2.0 bar discharge pressure due to reduced over-compression losses at 3.0bar discharge pressure. This further supports that the variable pitch rotors are more suitable for high pressure applications.

Variable profile rotors show lower volumetric efficiency as compared to uniform rotors due to smaller capacity of the machine and also higher internal pressure rise. The over-compression before discharge results in lower adiabatic efficiency except at 3.0bar discharge pressure where it is comparable with uniform rotors.

6 Conclusion

3D CFD grid generation for twin screw compressors with variable pitch and variable profile rotors was formulated and implemented. Examples of grids with variable geometries have been presented and CFD analysis has shown the flow characteristics in the machines.

From the numerical analysis presented here, flow advantages identified with variable geometry rotors were evaluated. The analysis showed that by varying the rotor lead continuously from the suction to the discharge ends, it is possible to improve compression characteristics with a steeper internal pressure build up. The analysis also showed that varying the rotor lead allows a larger size of discharge port area, thereby reducing throttling losses, and provides increase in volumetric efficiency by reducing the sealing line length in the high pressure zone. Analysis of variable profile rotors also showed the steeper internal pressure rise but there was no gain in

sealing line length and blow-hole area with this size of the rotors. The increase in root diameter of the female rotors with variable profile certainly helps in producing stiff rotors for high pressure applications.

These grid generation developments open new opportunities for further investigation of the flow behaviour and improvements in the performance of these machines by the use of CFD.

References

1. ANSYS 13.0, User Guide and Help Manual, 2011.
2. P.R. Eiseman, Control Point Grid Generation, *Computers & Mathematics with Applications,* 1992; **24**, No.5/6, 57-67.
3. P.R. Eiseman, J. Hauser, J.F. Thompson and N.P. Weatherill, Numerical Grid Generation in Computational Field Simulation and Related Fields, *Proceedings of the 4th International Conference*, Pineridge Press, Swansea, Wales, UK, 1994.
4. J.H. Ferziger and M. Peric, Computational Methods for Fluid Dynamics, ISBN 978-3-540-42074-3, Springer, Berlin, Germany, 1996.
5. J.S. Fleming and Y. Tang, The Analysis of Leakage in a Twin Screw Compressor and its Application to Performance Improvement, *Proceedings of IMechE, Part E, Journal of Process Mechanical Engineering*, 1994; **209**, 125.
6. J.S. Fleming, Y. Tang and G. Cook, The Twin Helical Screw Compressor, *Part 1*: Development, Applications and Competitive Position, *Part 2*: A Mathematical Model of the Working process, *Proc. Inst. Mech. Eng. Part C J. Mech. Eng. Sci.*, 1998; **212**, 369.
7. J.W. Gardner, US Patent No 3,424,373 – Variable Lead Compressor. Patented 1969.
8. K. Hanjalic and N. Stosic, Development and Optimization of Screw machines with a simulation Model – Part II: Thermodynamic Performance Simulation and Design Optimization. ASME Transactions. *Journal of Fluids Engineering.* 1997; **119**, 664.
9. J.H. Kim and J.F. Thompson, Three-Dimensional Adaptive Grid generation on a Composite-Block Grid, *AIAA Journal*, 1990; **28**, 3, 470-477.

10. A. Kovacevic, N. Stosic and I.K. Smith, Development of CAD-CFD Interface for Screw Compressor Design, *International Conference on Compressors and Their Systems, London, IMechE Proceedings*, 1999; **757**.
11. A. Kovacevic, N. Stosic and I.K. Smith, Grid Aspects of Screw Compressor Flow Calculations, *Proceedings of the ASME Advanced Energy Systems Division*, 2000; **40**, 83.
12. A. Kovacevic, Three-Dimensional Numerical Analysis for Flow Prediction in Positive Displacement Screw Machines, Ph.D. Thesis, School of Engineering and Mathematical Sciences, City University London, UK, 2002.
13. A. Kovacevic, N. Stosic and I.K. Smith, Numerical Simulation of Fluid Flow and Solid Structure in Screw Compressors, *Proceedings of ASME Congress, New Orleans, IMECE* 2002; **33367**.
14. A. Kovacevic, N. Stosic and I.K. Smith, 3-D Numerical Analysis of Screw Compressor Performance, *Journal of Computational Methods in Sciences and Engineering*, 2003; **3**, 2, 259-284.
15. A. Kovacevic, N. Stosic and I.K. Smith, A numerical study of fluid–solid interaction in screw compressors. *International Journal of Computer Applications in Technology*. 2004; **21**, 4, 148 – 158.
16. A. Kovacevic, Boundary Adaptation in Grid Generation for CFD Analysis of Screw Compressors, *Int. J. Numer. Methods Eng.*, 2005; **64**, 3, 401-426.
17. A. Kovacevic, N. Stosic and I.K. Smith, Numerical simulation of combined screw compressor–expander machines for use in high pressure refrigeration systems, *Simulation Modeling Practice and Theory*, 2006; **14**, 8, 1143–115.

18. A. Kovacevic, N. Stosic and I.K. Smith. *Screw compressors - Three dimensional computational fluid dynamics and solid fluid interaction*, ISBN 3-540-36302-5, Springer-Verlag Berlin Heidelberg New York, 2007.
19. V.D. Liseikin, Algebraic Adaptation Based on Stretching Functions, *Russian Journal for Numerical and Analytical Mathematical Modeling*, 1998; **13**, 4, 307-324.
20. V.D. Liseikin, Grid Generation Methods, ISBN 3-540-65686-3, Springer-Verlag (1999).
21. B.G. Prasad, CFD for Positive Displacement Compressors, *Proc. Int. Compressor Conf. at Purdue.* 2004; **1689**.
22. S. Rane, A. Kovacevic, N. Stosic and M. Kethidi, Grid Deformation Strategies for CFD Analysis of Screw Compressors, *Int Journal of Refrigeration*, http://dx.doi.org /10.1016/j.ijrefrig.2013.04.008, 2013.
23. A.J. Samareh and R.E. Smith, A Practical Approach to Algebraic Grid Adaptation, *Computers & Mathematics with Applications*, 1992; **24**, 5/6, 69-81.
24. T.I.P. Shih, R.T. Bailey, H.L. Ngoyen and R.J. Roelke, Algebraic Grid Generation For Complex Geometries, *Int. J. Numer. Meth. Fluids*, 1991; **13**, 1-31.
25. B.K. Soni, Grid Generation for Internal Flow Configurations, *Computers & Mathematics with Applications*, 1992; **24**, 5/6, 191-201.
26. E. Steinthorsson, T.I.P. Shih and R.J. Roelke, Enhancing Control of Grid Distribution In Algebraic Grid Generation, *Int. J. Numer. Meth. Fluids*, 1992; **15**, 297-311.
27. N. Stosic, On Gearing of Helical Screw Compressor Rotors, *Journal of Mechanical Engineering Science*, 1998; **212**, 587.
28. N. Stosic, I.K. Smith and A. Kovacevic, *Screw Compressors: Mathematical Modeling and Performance Calculation*, Springer Verlag, Berlin, ISBN: 3-540-24275-9, 2005.

29. J.F. Thompson, Grid Generation Techniques in Computational fluid Dynamics, *AIAA Journal*, 1984; **22**, 11, 1505-1523.
30. J.F. Thompson and B. Soni, Weatherill NP. Handbook of Grid generation, CRC Press, 1999.
31. J.V. Voorde, J. Vierendeels and E. Dick, Development of a Laplacian-based mesh generator for ALE calculations in rotary volumetric pumps and compressors. *Computer Methods in Applied Mechanics and Engineering*, 2004; **193**, 39–41, 4401-4415.
32. J.V. Voorde and J. Vierendeels, A grid manipulation algorithm for ALE calculations in screw compressors. *17th AIAA Computational Fluid Dynamics Conference*, Canada, AIAA 2005; **4701**.

Figure Captions

Deforming Grid Generation and CFD analysis of Variable Geometry Screw Compressors

Sham Rane*, Ahmed Kovacevic, Nikola Stosic, Madhulika Kethidi

Fig. 1. Oil free Twin Screw compressor and its working chamber

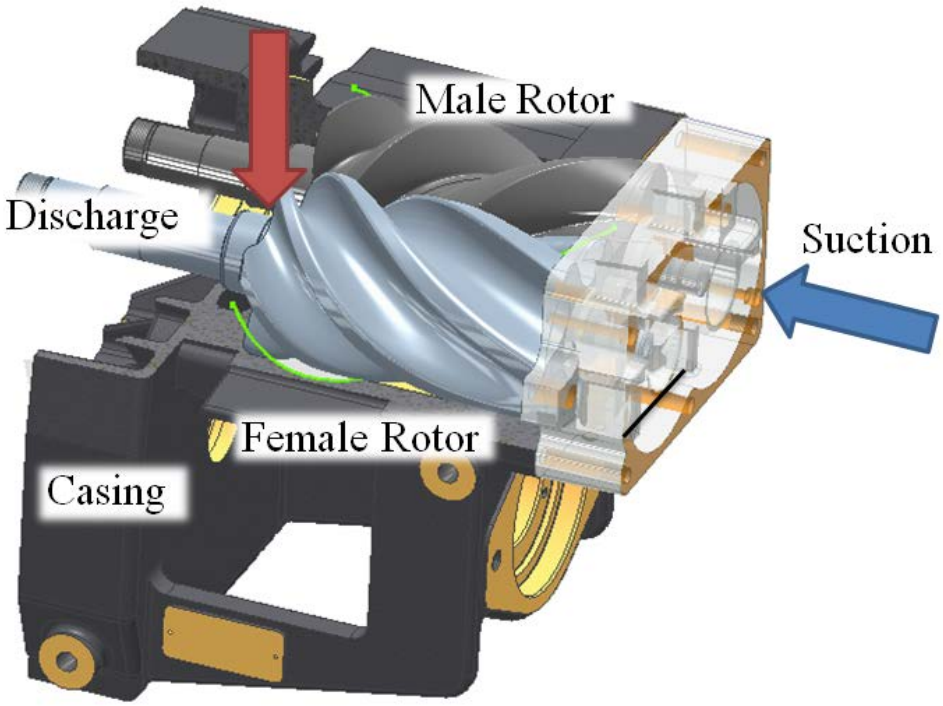

Fig. 2. Meshing of Uniform Pitch Twin Screw Rotors

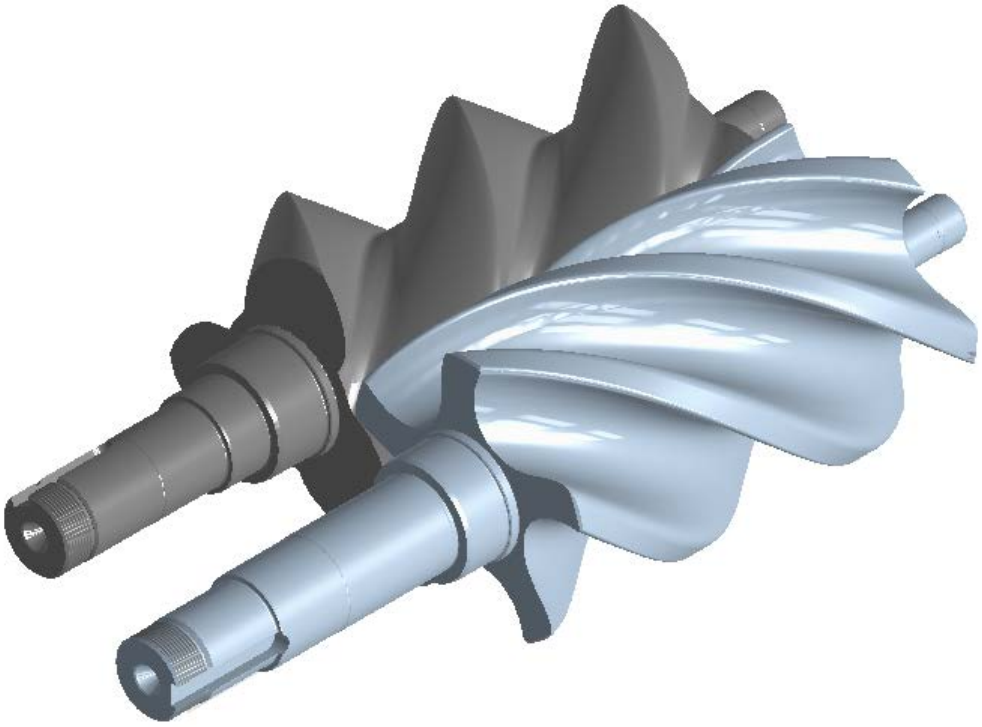

Fig. 3. Meshing of Variable Pitch Twin Screw Rotors

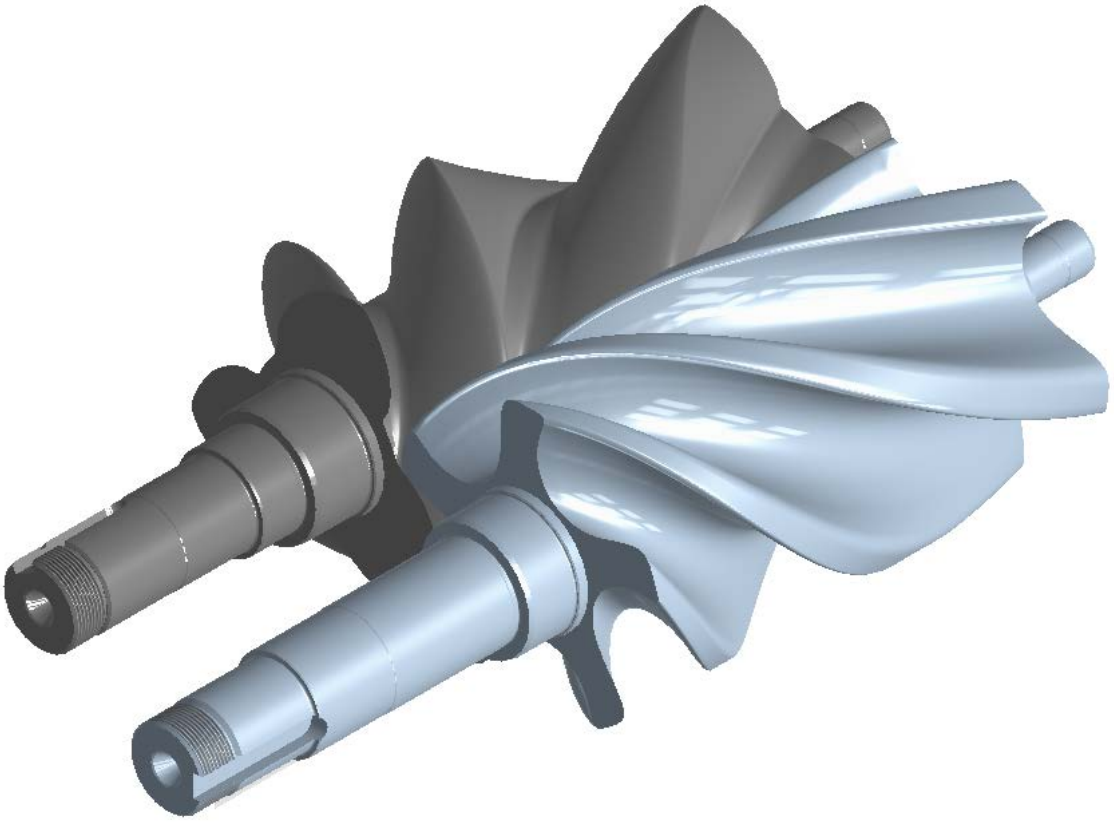

Fig. 4. Volume-Angle diagram

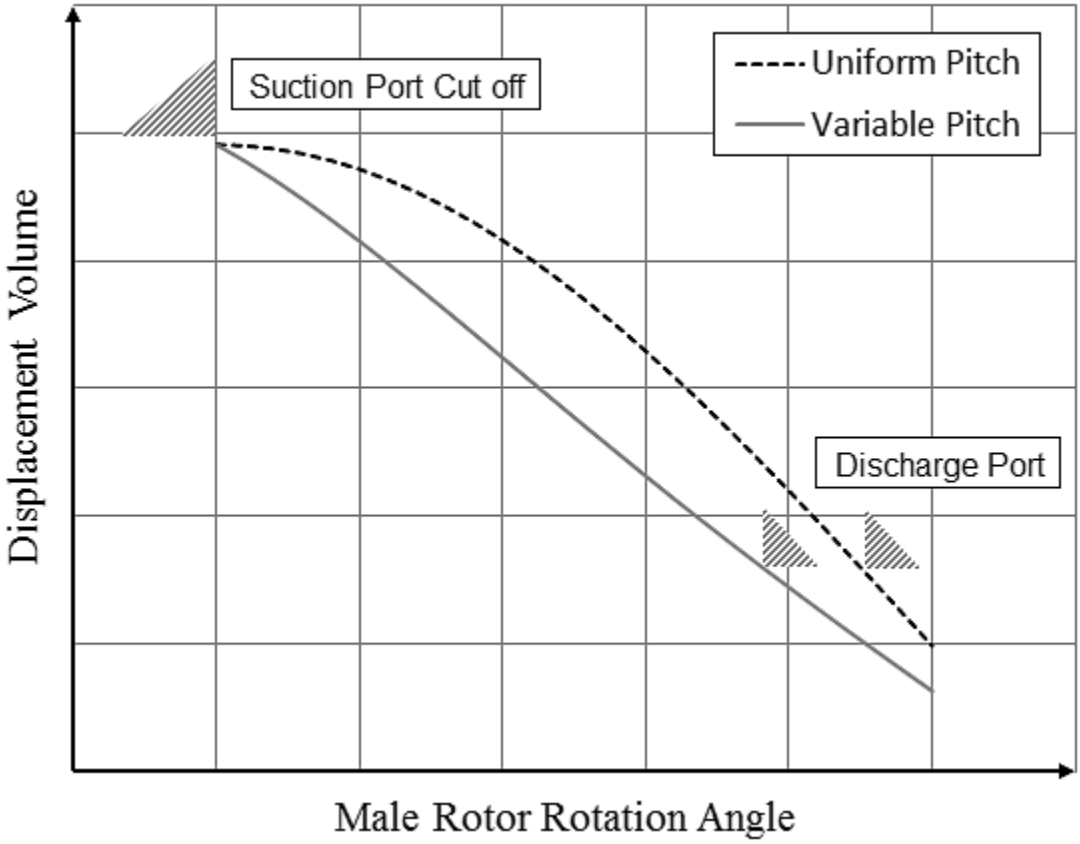

Fig. 5. Pressure-Angle Diagram

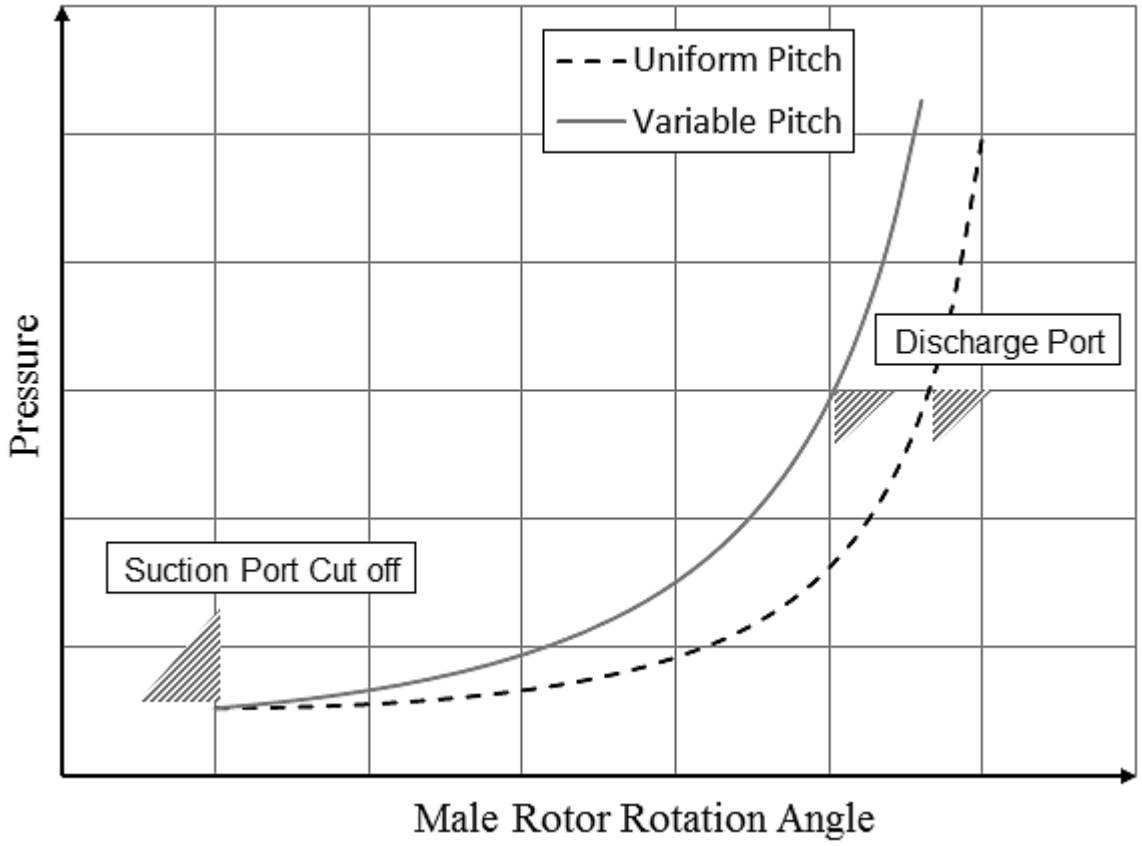

Fig. 6. Cylinder and Port development of a rotor pair

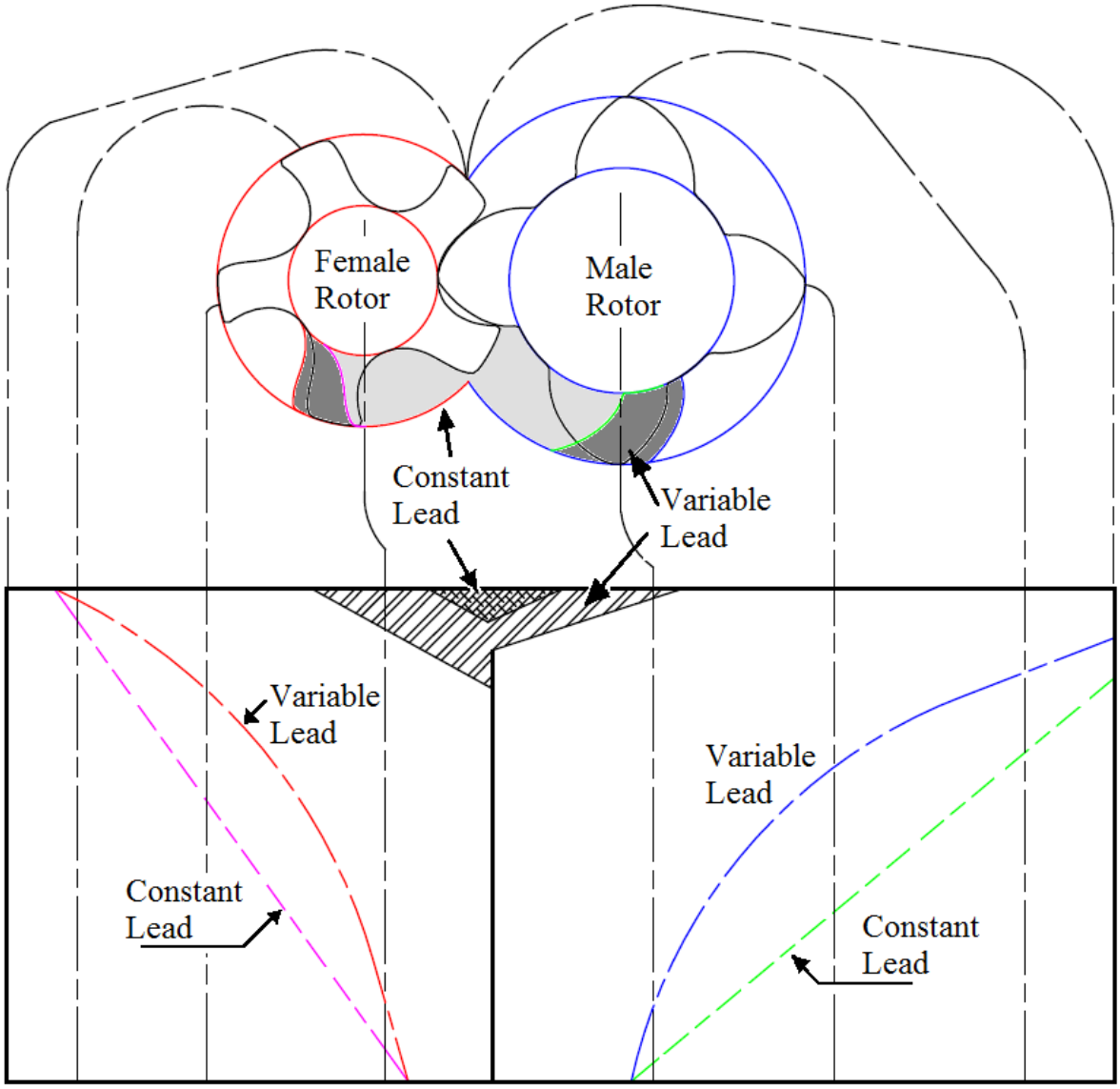

Fig. 7. Twin screw compressor working chamber domains

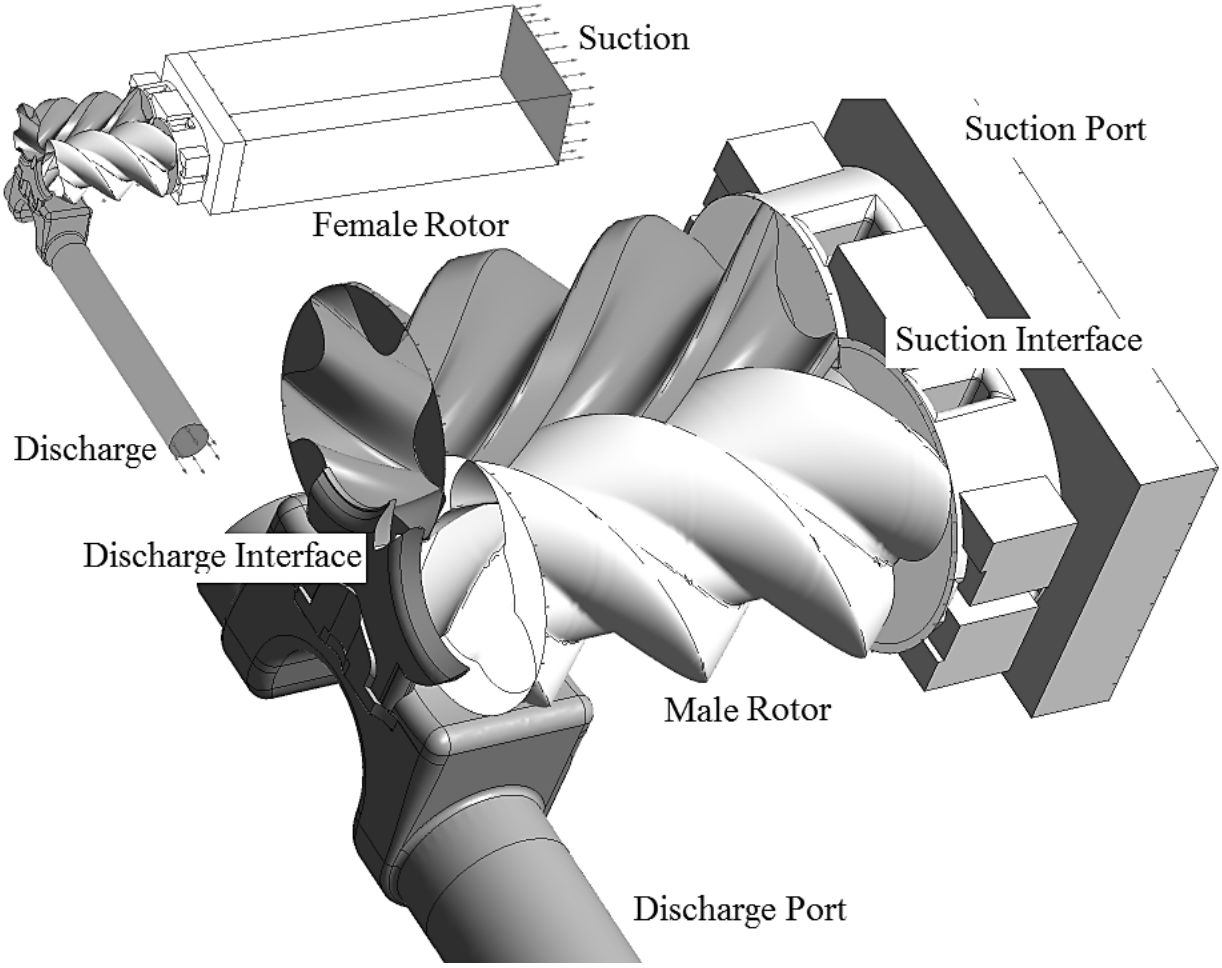

Fig. 8. Simplified Block Diagram of Screw Compressor Rotor Grid Generator

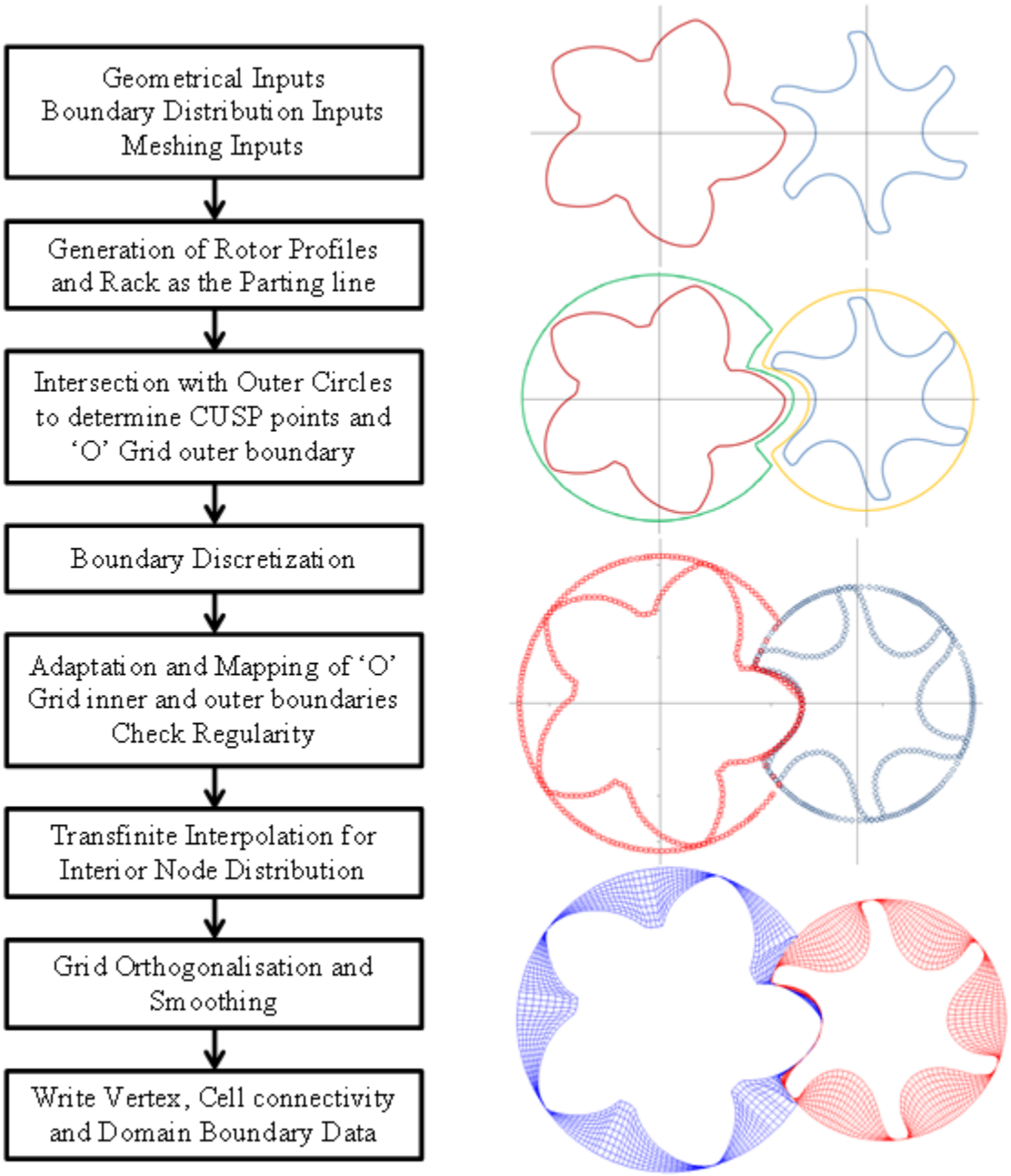

Fig. 9. Uniform Pitch Grid Generation

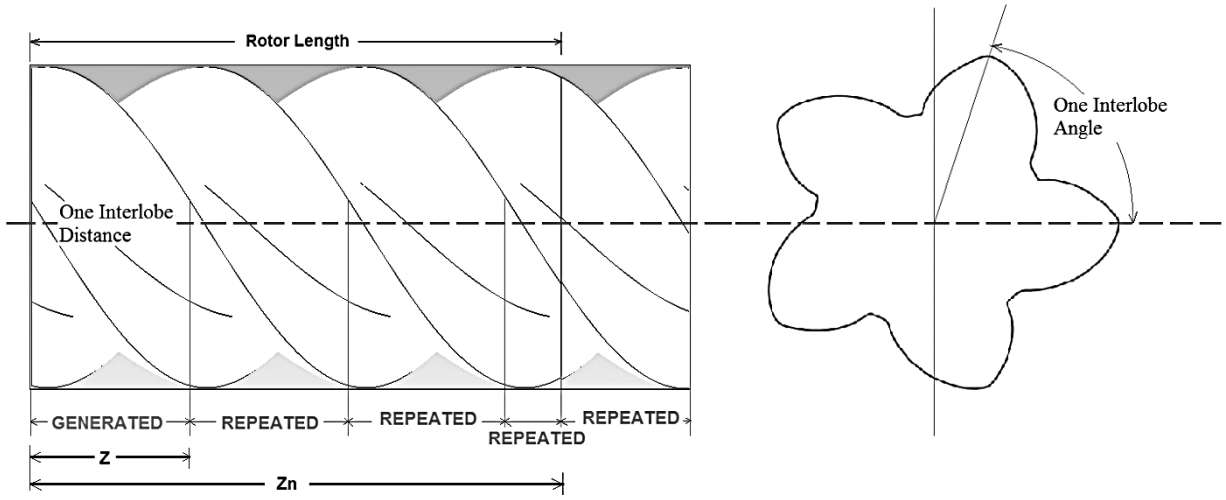

Fig. 10. Uniform Pitch Rotor Grid Assembly in 3D

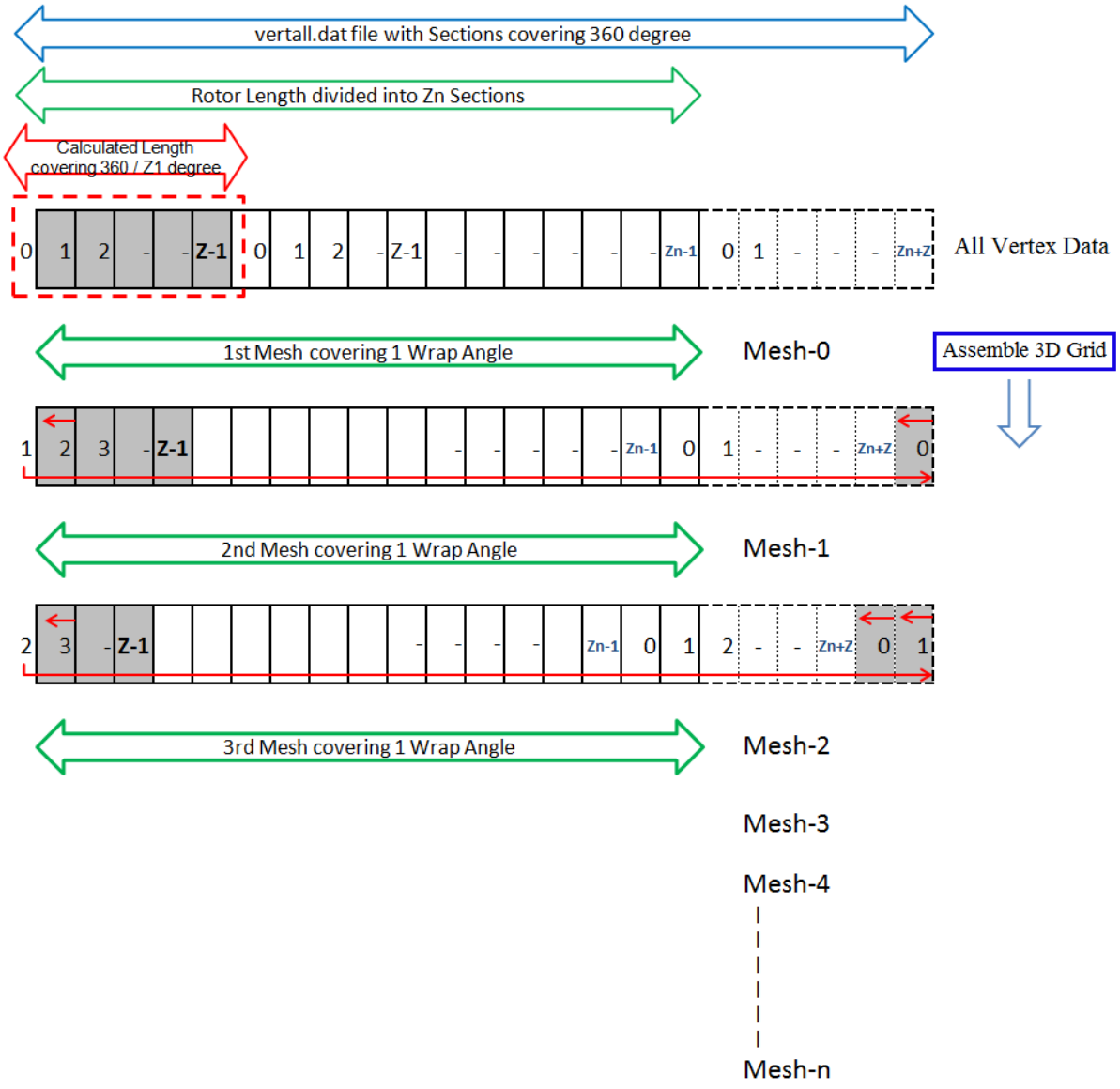

Fig. 11. Axial spacing difference between uniform pitch and variable pitch rotor grids

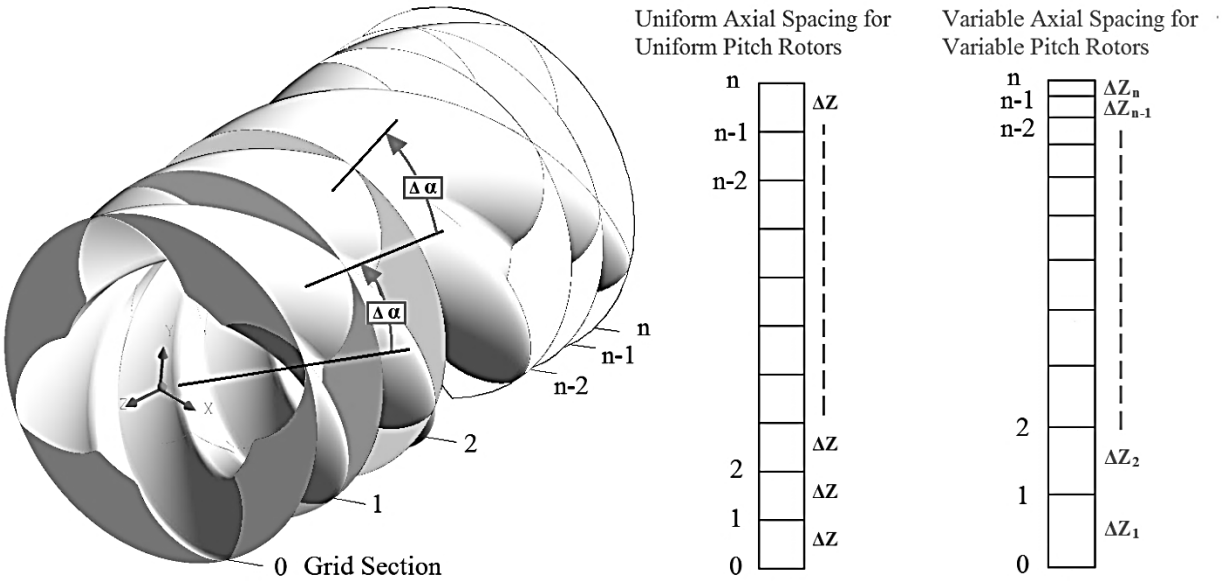

Fig. 12. Twin screw compressor rotor with variable section profile

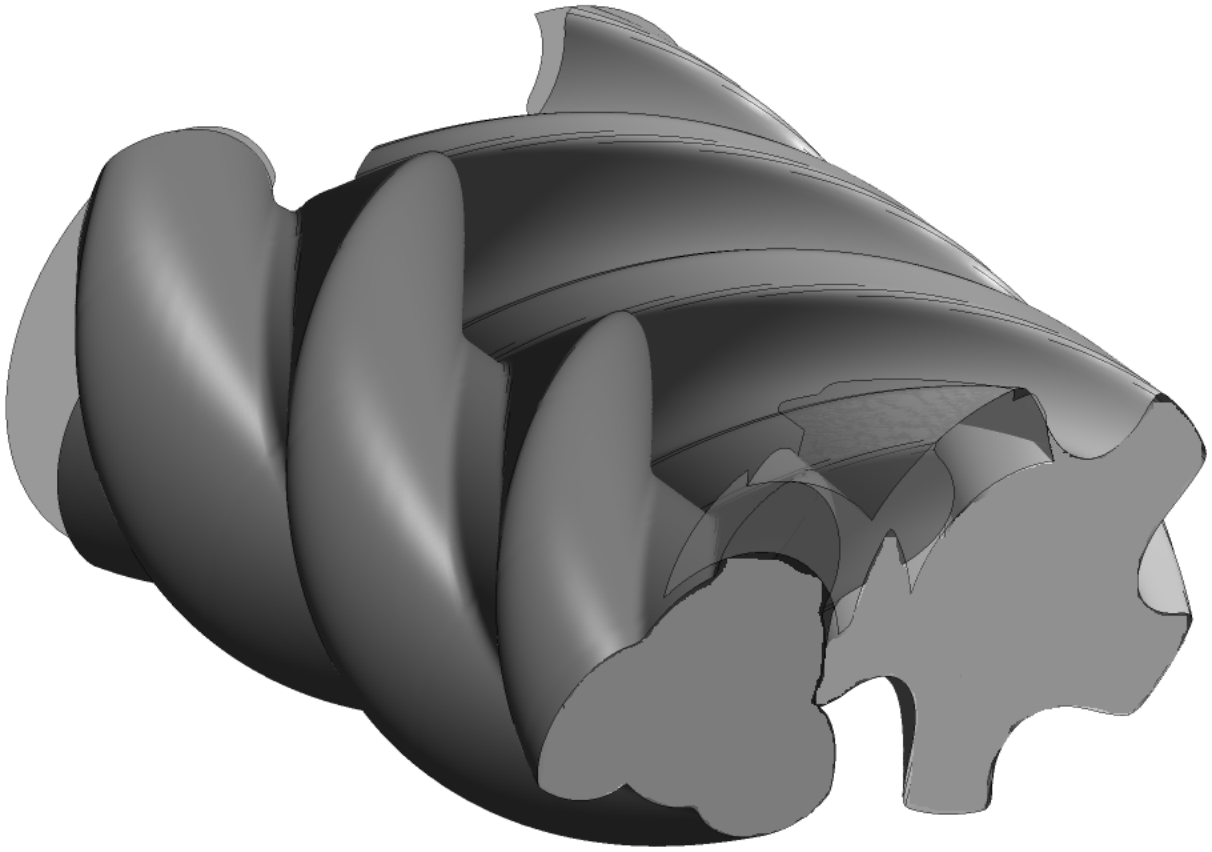

Fig. 13. Angular rotation of sections for different Pitch Functions

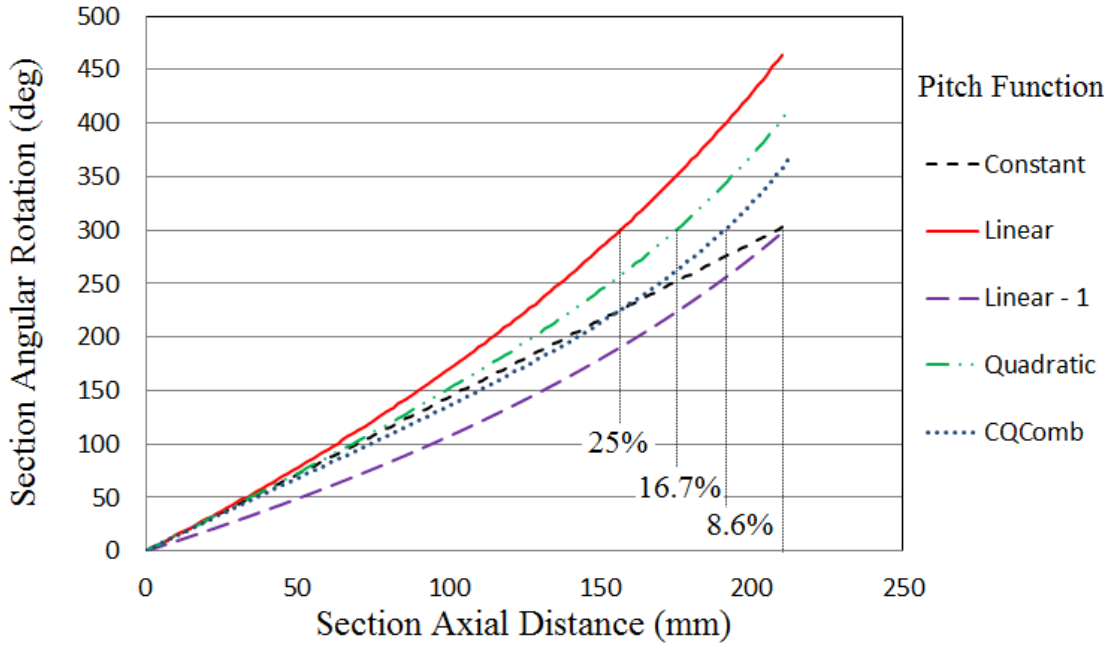

Fig. 14. Variable Pitch and Variable Profile Grid Generation

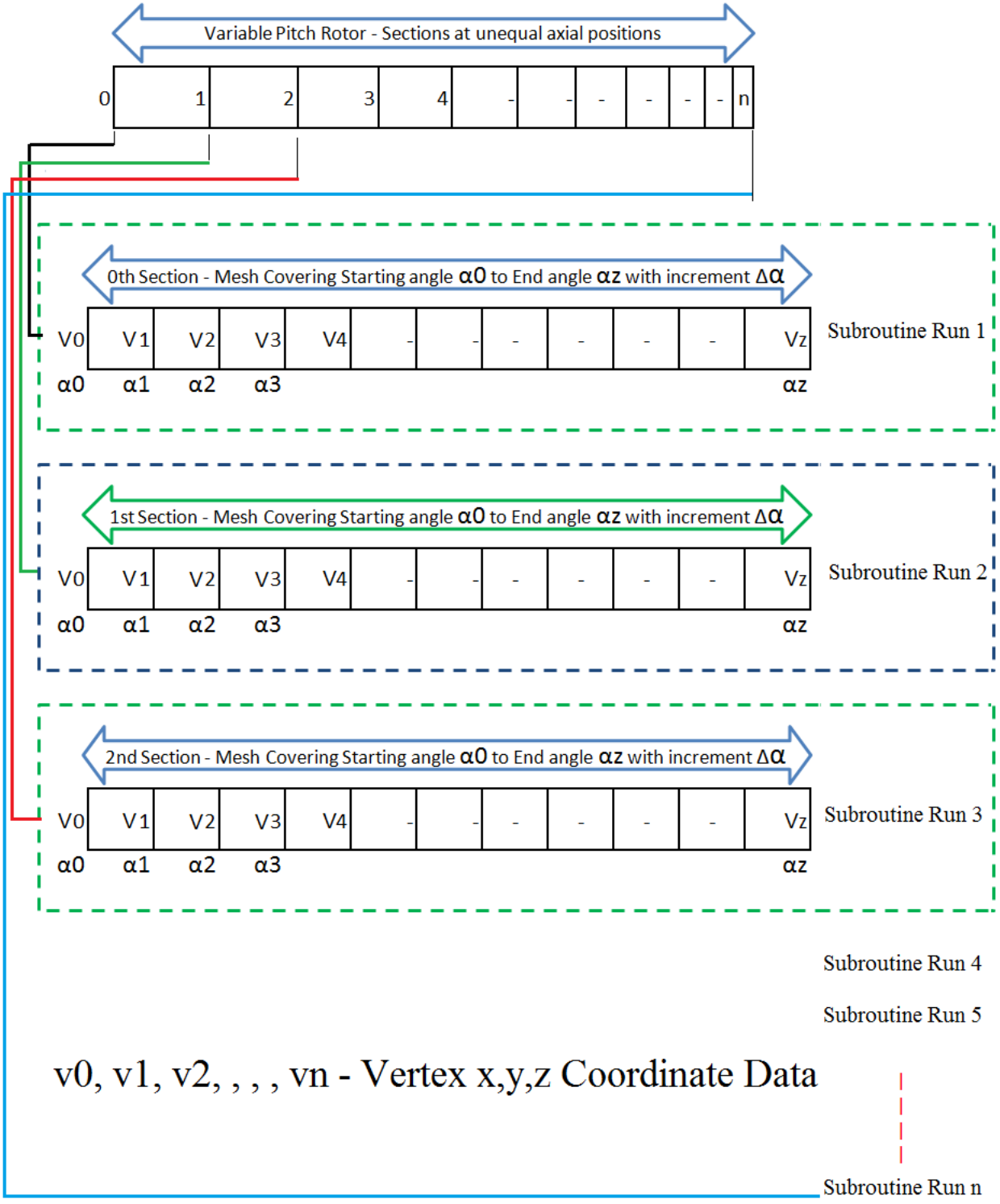

Fig. 15. Grid Assembly in 3D for Variable Pitch and Variable Profile rotors

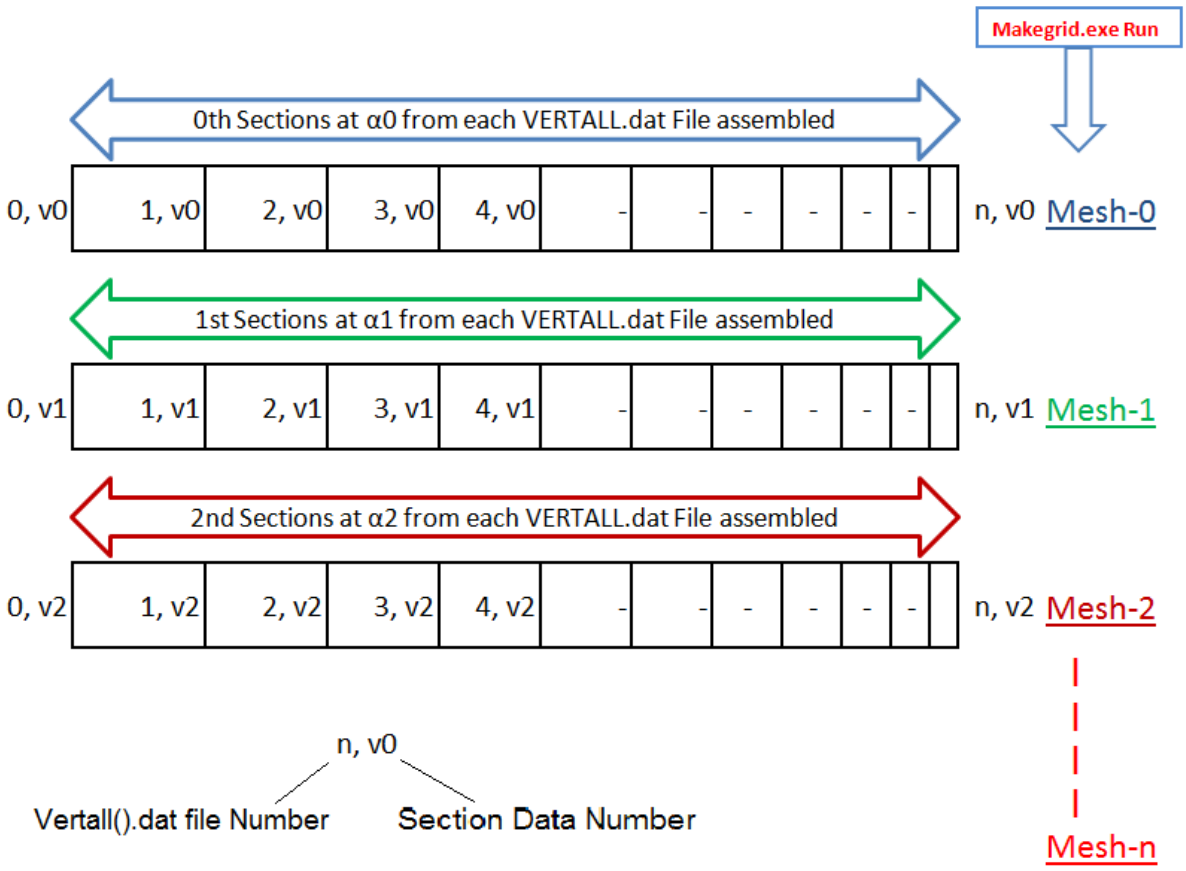

Fig. 16. Examples of variable pitch grid with uniform profile on 5/6 ‘N’ rotors

Constant Lead Pitch = 50.46mm	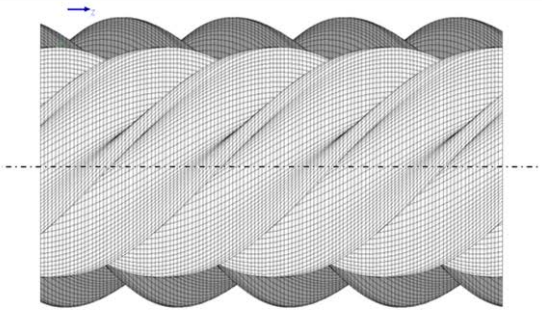	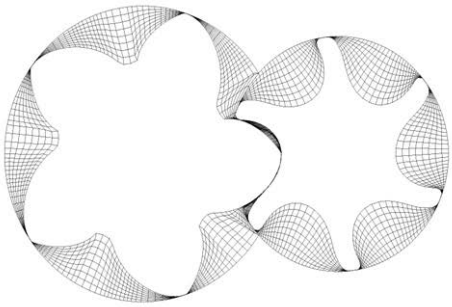
Linear Pitch variation Start Pitch 50.46mm End Pitch 20.00 mm	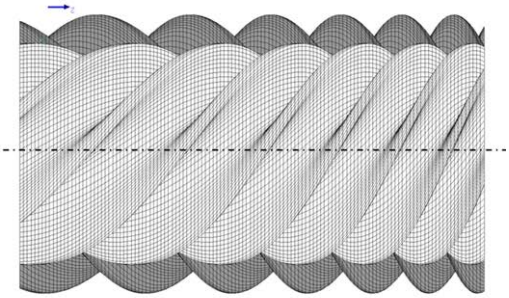	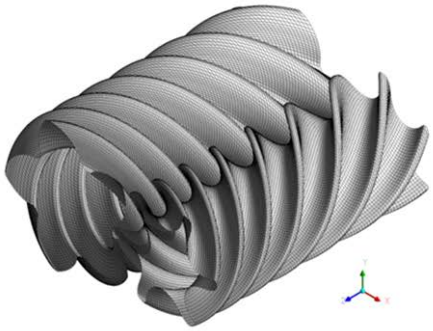
Linear Pitch variation Start Pitch 80.00mm End Pitch 20.00 mm	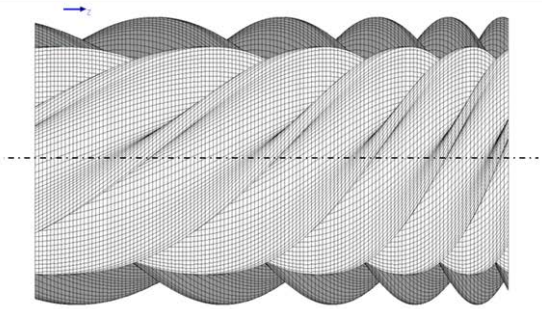	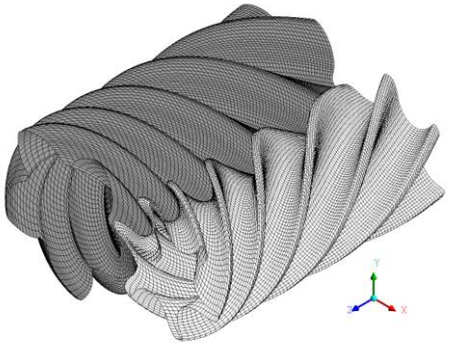

Fig. 17. Example of a uniform pitch grid with a variable profile on 3/5 ‘Rotor Generated N’ rotors

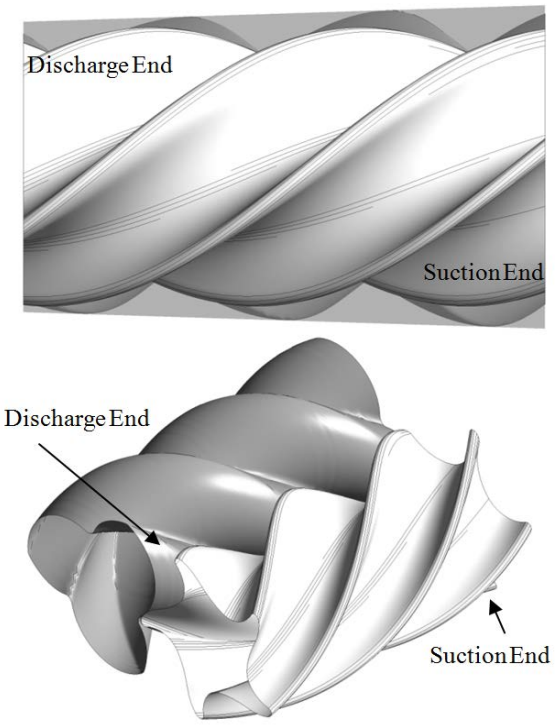

Fig. 18. Grid sections of variable geometry on 3/5 ‘Rotor Generated N’ rotors

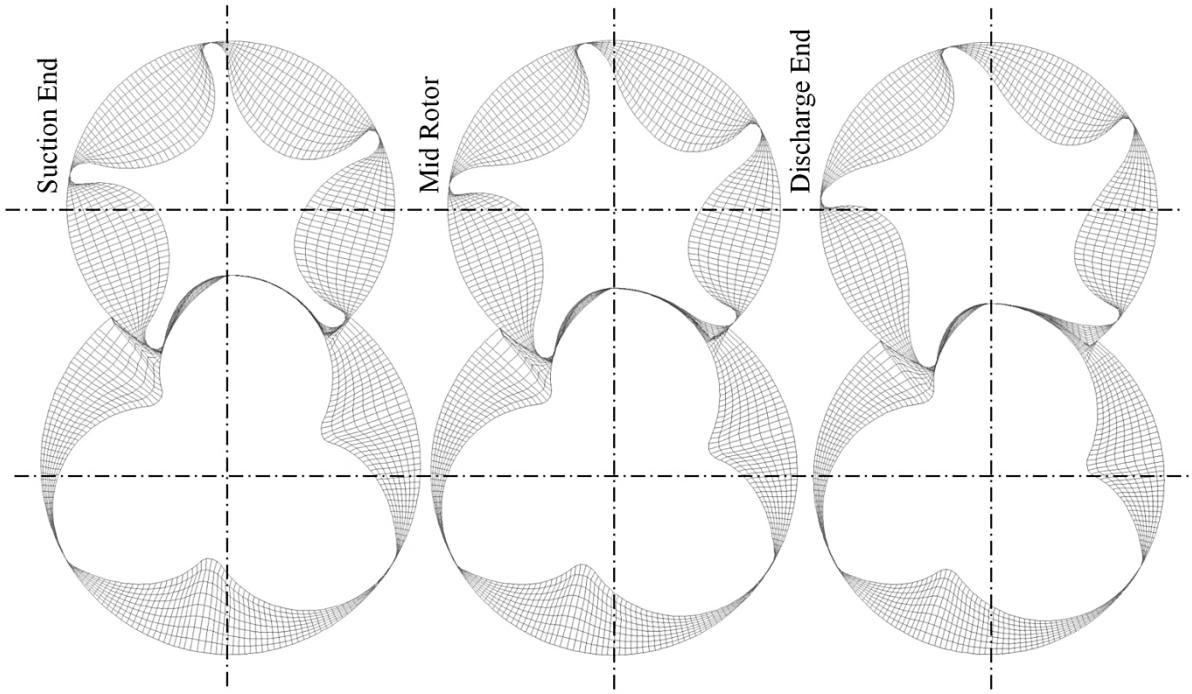

Fig. 19. Reduced discharge port area in *Case 2* compared with *Case 1*

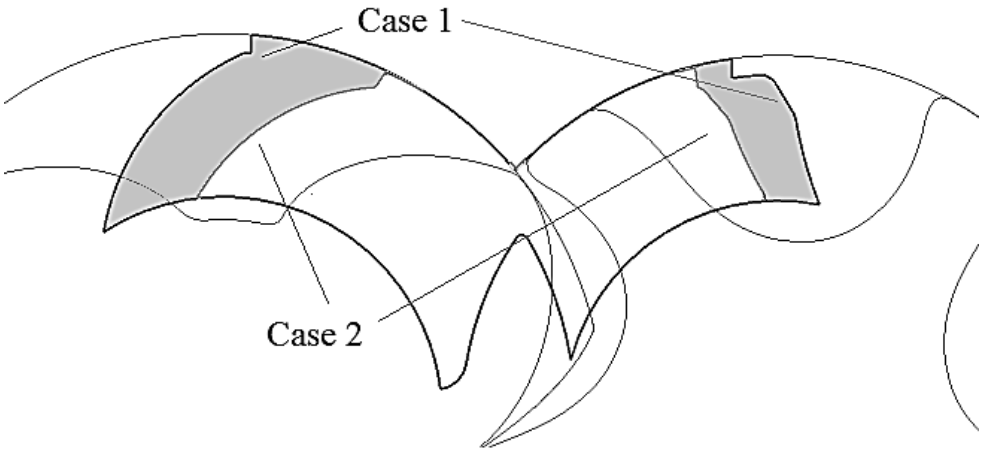

Fig. 20. Variable pitch grid – 3/5 ‘N’ rotors

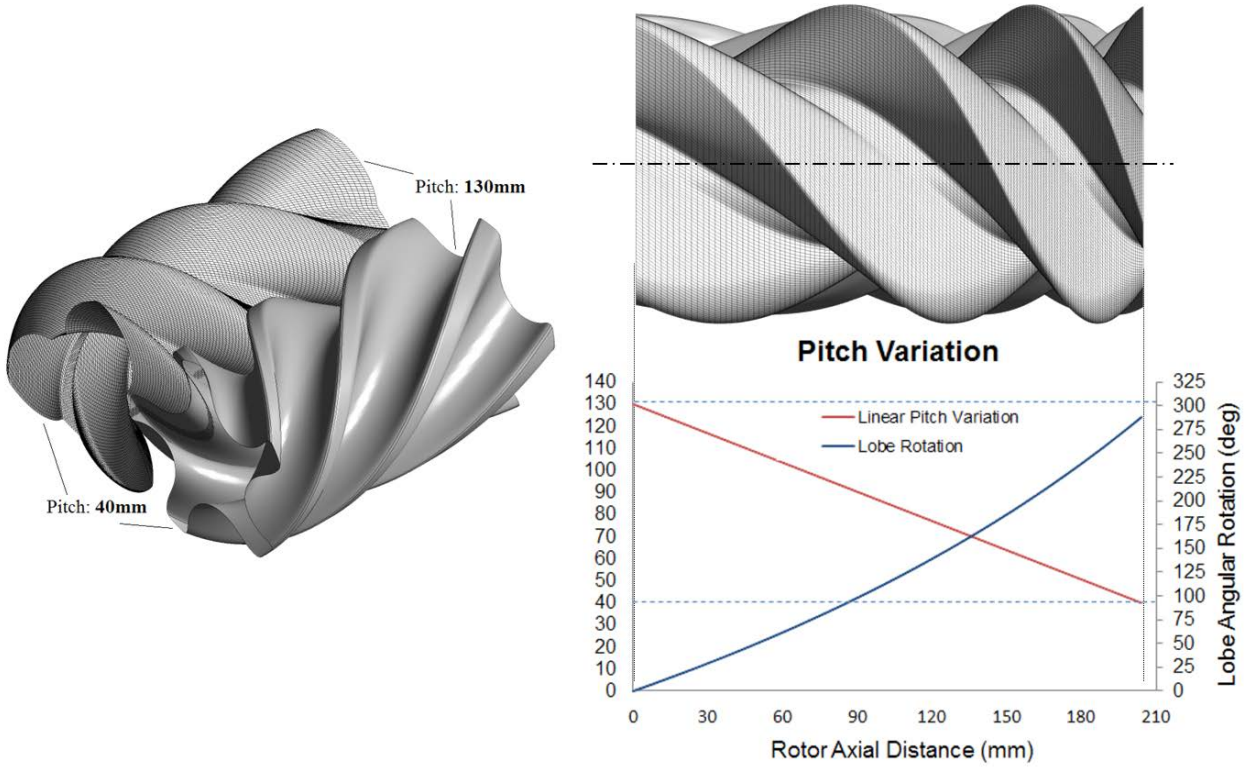

Fig. 21. Variable profile grid – 3/5 ‘N’ rotors

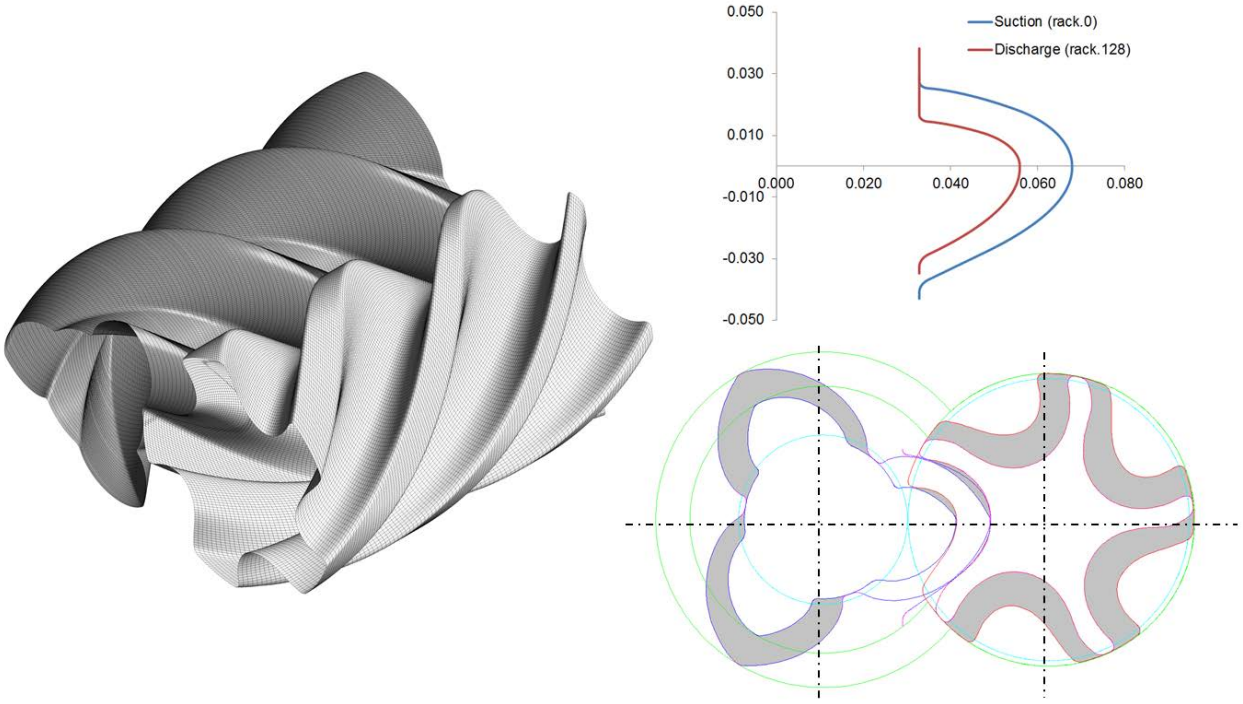

Fig. 22. Different level of grid refinements shown for one section

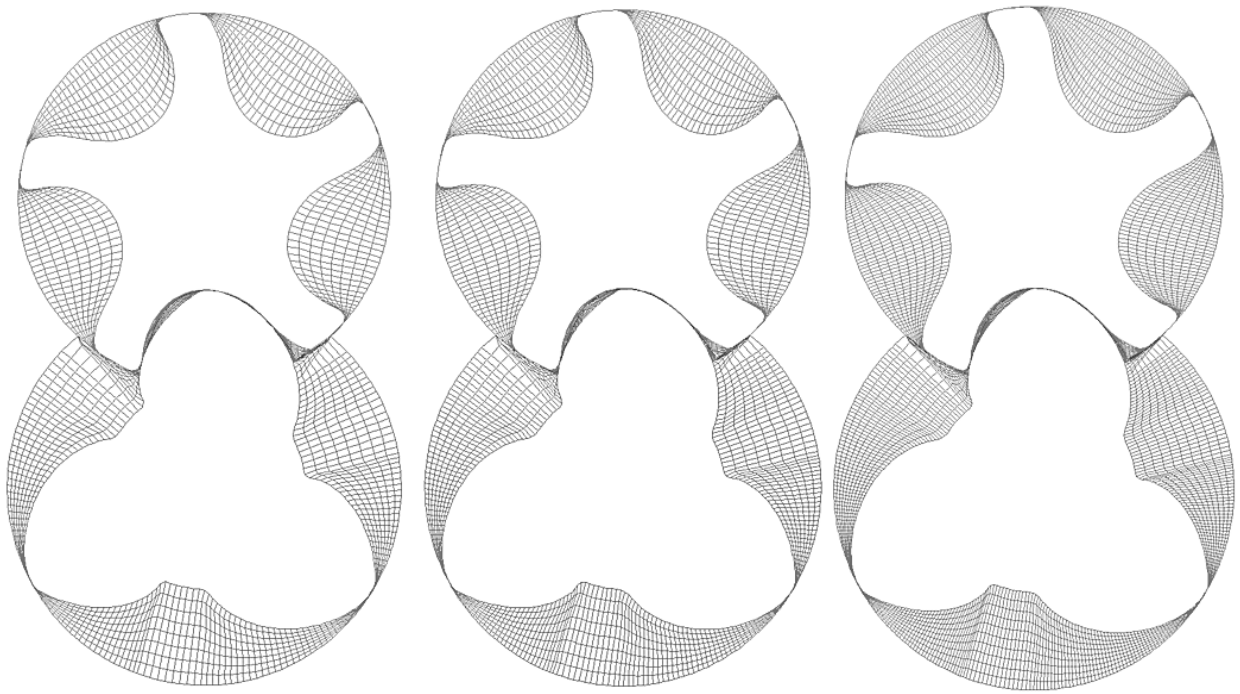

Fig. 23. Pressure variation on variable pitch medium grid case with discharge pressure 2.0bar.

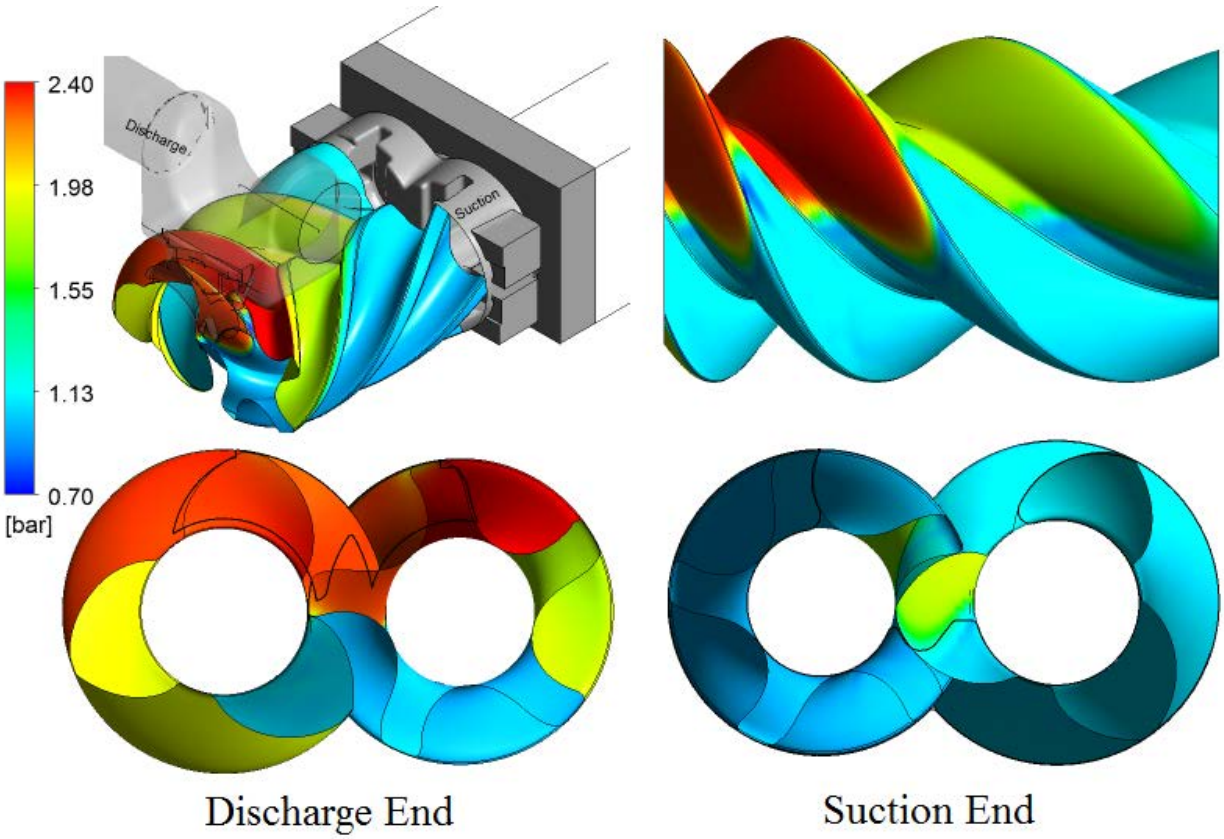

Fig. 24. Indicator diagram for cases calculated on fine grid. Discharge pressure 2.0 bar.

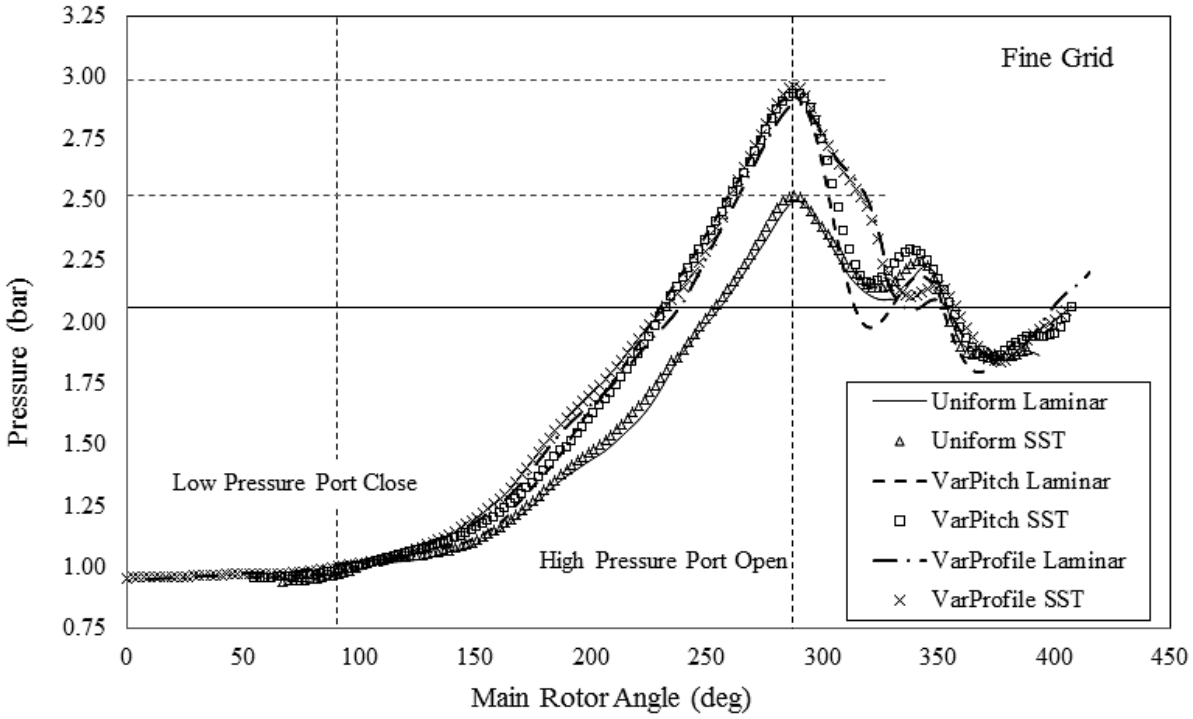

Fig. 25. Indicator diagram for cases calculated on fine grid with turbulence models. Discharge pressure 2.0bar and 3.0 bar

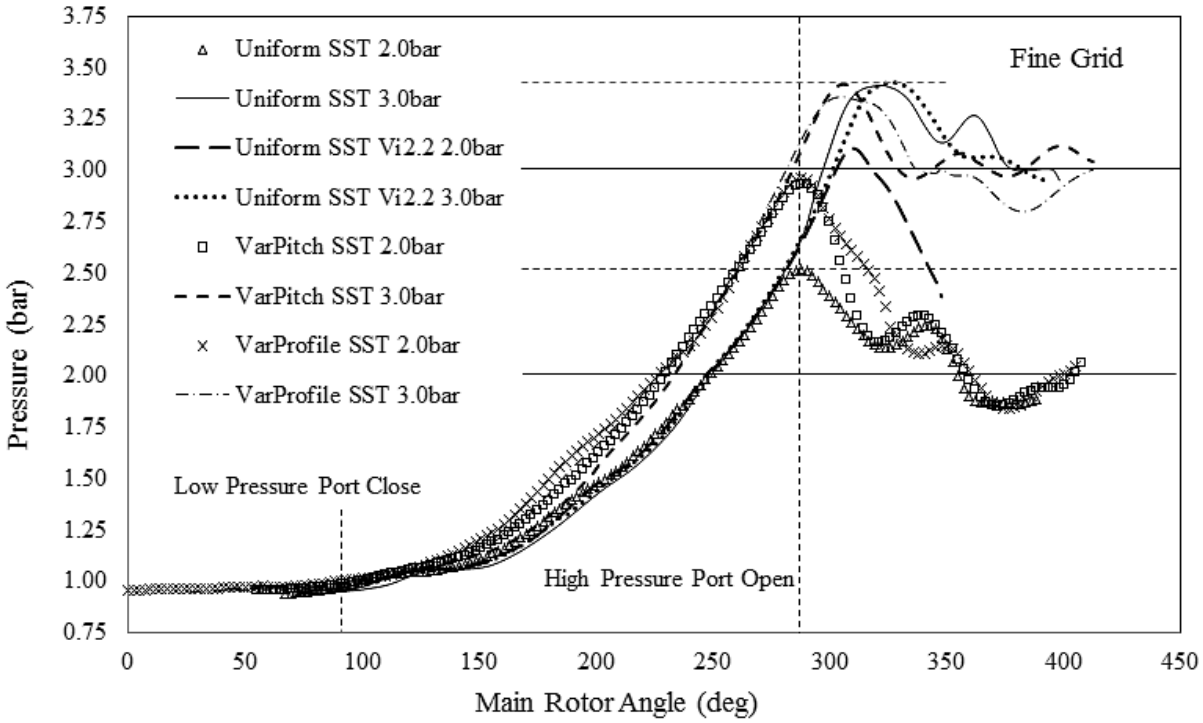

Fig. 26. Effect of grid refinement on integral parameters in cases 1,3 and 4 with 2.0bar discharge pressure

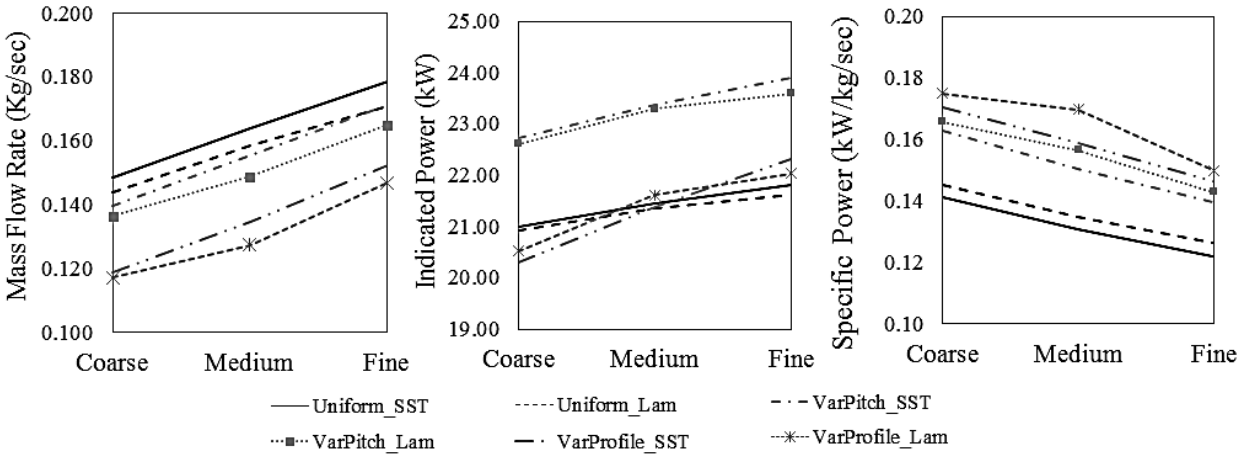

Fig. 27. Indicator diagram for cases 4 showing effect of grid refinement with 2.0bar discharge pressure

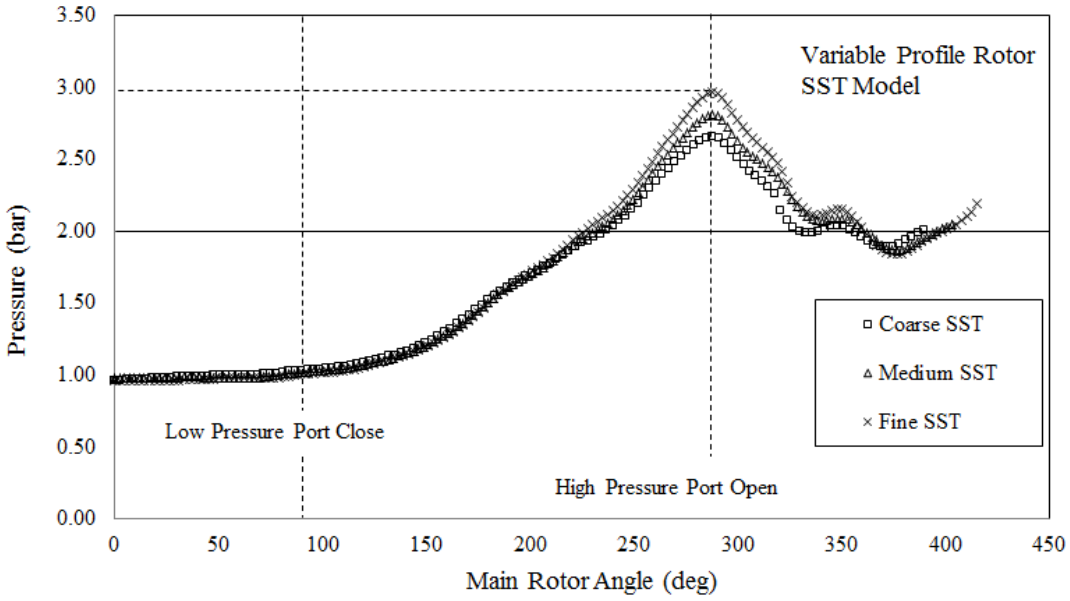

Fig. 28. Comparison of interlobe sealing line lengths

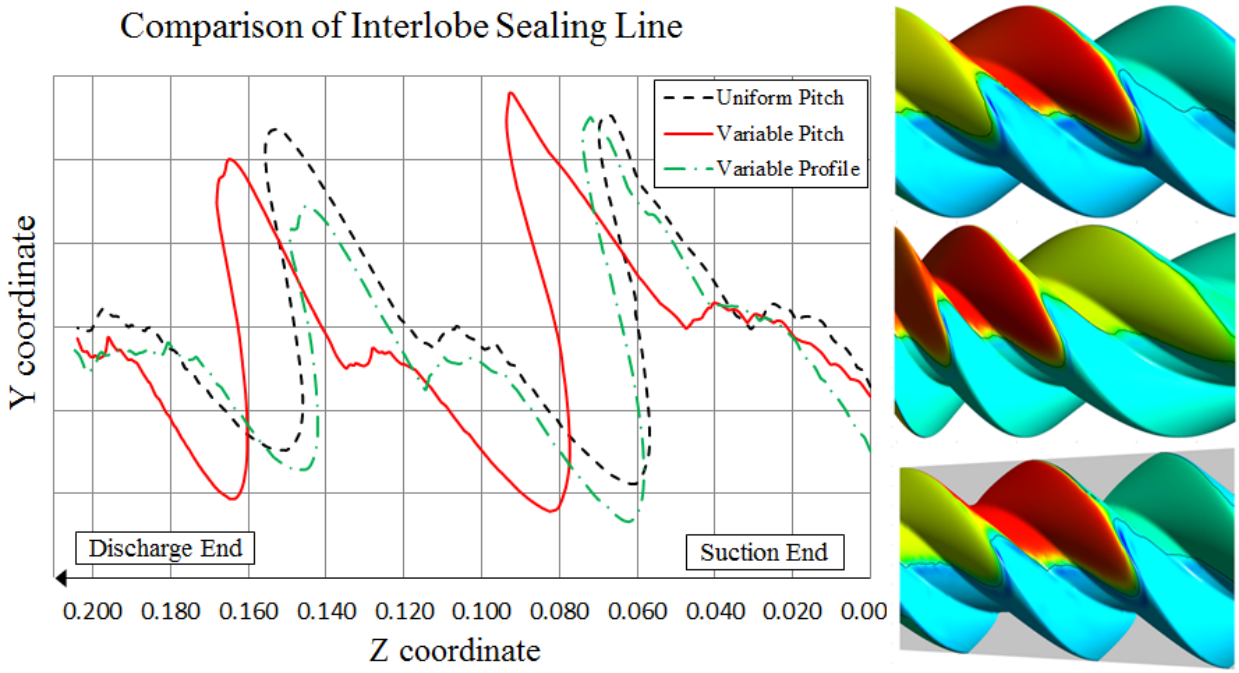

Fig. 29. Comparison of Blow-hole area

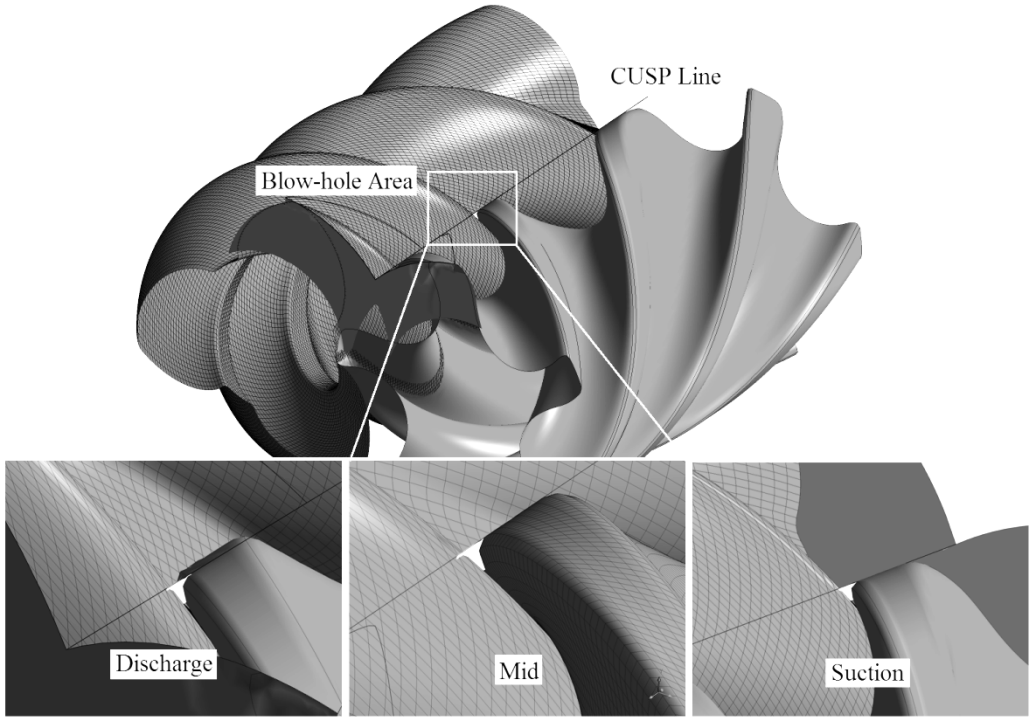

Fig. 30. Comparison of performance at 2.0bar and 3.0bar discharge pressure with fine grid cases

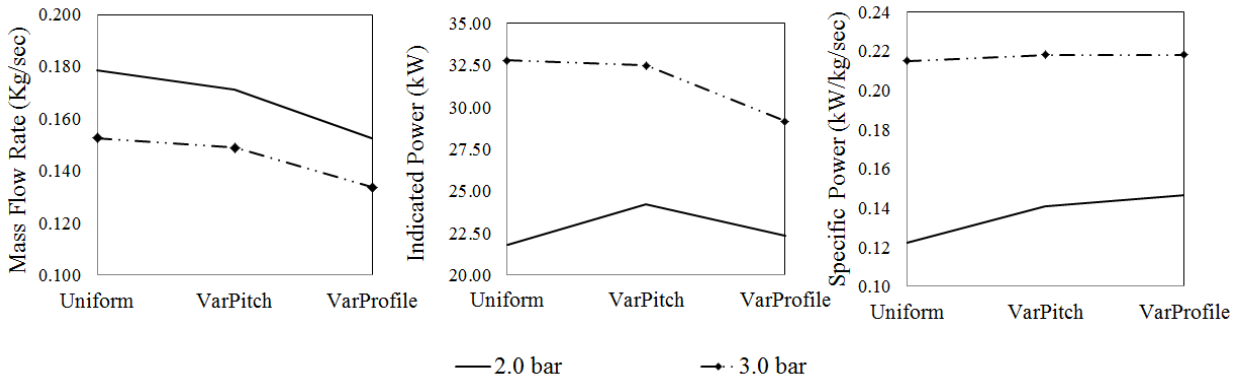
Mass Flow Rate (Kg/sec)
0.200
0.180
0.160
0.140
0.120
0.100
Uniform
VarPitch
VarProfile
Indicated Power (kW)
35.00
32.50
30.00
27.50
25.00
22.50
20.00
Uniform
VarPitch
VarProfile
Specific Power (kW/kg/sec)
0.24
0.22
0.20
0.18
0.16
0.14
0.12
0.10
Uniform
VarPitch
VarProfile
2.0 bar
3.0 bar

Table 1 Grid refinement as number of computational nodes

Case	Uniform	Variable Pitch	Variable Profile
Coarse	691174	648190	675918
Medium	838378	915184	889794
Fine	1214418	1344944	1297434

Table 2 Comparison of Interlobe Sealing Line Length [mm]

Interlobe No	Uniform	Variable Pitch	Difference	Var. Prof	Difference
1	145.8	175.9	-30.1	158.4	-12.6
2	170.3	164.0	+6.4	162.2	+08.1
3 (part)	069.1	056.8	+12.2	068.4	+00.6
Total	385.2	396.6	-11.5	389.1	-03.9

Table 3 Comparison of Blow-hole area [mm^2]

Position	Uniform	Var. Pitch	Diff %	Var. Profile	Diff %
Suction	9.817	12.49	-27.2	9.83	-0.15
Mid	9.908	9.263	6.51	9.35	5.64
Discharge	9.701	6.562	32.3	9.19	5.29

Table 4 Comparison of predicted variable geometry rotor efficiencies

		Volumetric Efficiency %		Adiabatic Efficiency %	
		2.0 bar	**3.0 bar**	**2.0 bar**	**3.0 bar**
Uniform	Vi 1.8	75.30	56.70	54.13	51.73

Uniform	Vi 2.2	64.00	55.66	44.06	49.91
Variable Pitch	Vi > 1.8	66.20	57.60	46.88	50.99
Variable Profile	Vi > 1.8	62.80	55.04	45.16	51.01